A STABILIZED TRACE FINITE ELEMENT METHOD FOR PARTIAL DIFFERENTIAL EQUATIONS ON EVOLVING SURFACES[*]

CHRISTOPH LEHRENFELD[†], MAXIM A. OLSHANSKII[‡], AND XIANMIN XU[§]

Abstract. In this paper, we study a numerical method for the solution of partial differential equations on evolving surfaces. The numerical method is built on the stabilized trace finite element method (TraceFEM) for the spatial discretization and finite differences for the time discretization. The TraceFEM uses a stationary background mesh, which can be chosen independent of time and the position of the surface. The stabilization ensures well-conditioning of the algebraic systems and defines a regular extension of the solution from the surface to its volumetric neighborhood. Having such an extension is essential for the numerical method to be well-defined. The paper proves numerical stability and optimal order error estimates for the case of simplicial background meshes and finite element spaces of order $m \geq 1$. For the algebraic condition numbers of the resulting systems we prove estimates, which are independent of the position of the interface. The method allows that the surface and its evolution are given implicitly with the help of an indicator function. Results of numerical experiments for a set of 2D evolving surfaces are provided.

Key words. surface PDEs, evolving surfaces, TraceFEM, level set method

AMS subject classifications. 65M60, 58J32

1. Introduction. Partial differential equations on evolving surfaces arise in a number of mathematical models in natural sciences and engineering. Well-known examples include the diffusion and transport of surfactants along interfaces in multiphase fluids [18, 30, 42], diffusion-induced grain boundary motion [5, 28] and lipid interactions in moving cell membranes [11, 32]. Thus, recently there has been a significant interest in developing and analyzing numerical methods for PDEs on time-dependent surfaces; see, for example, the review articles [10, 34]. The present paper contributes to the field with an unfitted finite element methods for PDEs posed on implicitly defined time-dependent surfaces and its complete stability and error analysis.

Geometrically unfitted finite element methods exploit the idea of using a time-independent background finite element space to approximate the solution of a PDE posed on an embedded surface. The background finite element space is defined on an ambient triangulation, which is not fitted to the surface. There are several approaches that fit this framework. In the PDE extension approach, one extends the PDE off the surface to a volumetric computational domain in a special way such that the solution of the ambient PDE restricted to the surfaces solves the original problem. Further one solves this new PDE by a conventional discretization method in $\mathbb{R}^3$; see [2], and [44] for the extension to evolving surface case. In the trace finite element method, one takes an opposite approach. Instead of extending the surface PDE, one takes the traces of the background volumetric finite element functions on the embedded surface for the purpose of PDE approximation [35]. In the TraceFEM, one also may add stabilization terms which involve the restrictions of the background functions to the tetrahedra cut by the surface [3]. Several authors have treated PDEs on time-dependent surfaces using this framework. Thus, a method based on a characteristic-Galerkin formulation combined with the TraceFEM in space was proposed in [21]. An interesting variant of TraceFEM and narrow-band FEM for a conservation law on an evolving surface was devised in [6]. A mathematically sound approach which entails rigorous stability and error analysis was investigate in [36, 33]. In those papers, a PDE on an evolving closed surface $\Gamma(t) \subset \mathbb{R}^3$ was studied as an equation posed on a fixed space–time manifold $\mathcal{G} = \bigcup_{t \in (0,T)} \Gamma(t) \times \{t\} \subset \mathbb{R}^4$. Further a space–time trace finite element method was applied to approximate the PDE posed on $\mathcal{G}$. While the space–time TraceFEM was shown to be provably accurate, its implementation requires the numerical integration over the time slices of $\mathcal{G}$.

[†]Institute for Numerical and Applied Mathematics, University of Göttingen, Göttingen, Germany, lehrenfeld@math.uni-goettingen.de, http://num.math.uni-goettingen.de/~lehrenfeld/

[‡]Department of Mathematics, University of Houston, Houston, Texas 77204-3008 molshan@math.uh.edu, http://www.math.uh.edu/~molshan/

[§]LSEC, Institute of Computational Mathematics and Scientific/Engineering Computing, NCMIS, AMSS, Chinese Academy of Sciences, Beijing 100190, China xmxu@lsec.cc.ac.cn.

An algorithm for piecewise tetrahedral reconstruction of $\mathcal{G}$ from the zero of a level-set function can be found in [15, 24], but these reconstruction methods are not a part of standard scientific computing software. Moreover, it remains a challenging problem to build a higher order reconstruction of $\mathcal{G}$. Recent attempts to build geometrically unfitted finite element method that avoids numerical recovery of $\mathcal{G}$ are reported in [22, 13, 39]. At time of writing this paper, the authors are unaware of stability or error analysis of any of these most recent methods. Therefore, building an accurate, efficient and reliable unfitted finite element method for PDEs posed on surfaces is still a challenge. In particular, one may want the method to benefit from higher order elements, to avoid a reconstruction of $\mathcal{G}$, and to admit rigorous analysis.

The present paper addresses the challenge by suggesting a hybrid finite difference (FD) in time / TraceFEM in space method, which uses the restrictions of surface independent background FE functions on a steady discrete surface $\Gamma_h(t_n)$ for each time node t_n. A standard FD approximation is applied to treat the time derivative. Hence, a reconstruction of $\mathcal{G}$ is not needed. Instead one needs an extension of the TraceFEM solution (but not of the PDE!) from $\Gamma_h(t_n)$ to a narrow band of tetrahedra containing $\Gamma_h(t_n)$. In [39] it was suggested that a quasi-normal extension of the discrete solution by a variant of the fast marching method (FMM) can be used allowing the modular application of the standard tools: steady-surface TraceFEM and FMM. Numerical experiments in [39] demonstrated that the piecewise linear TraceFEM combined with BDF2 in time and a variant of the FMM from [18] is second-order accurate for $h = \Delta t$, unconditionally stable and capable to handle the case of surfaces undergoing topological changes. Here we build on the approach from [39], with the following important modification: The finite element formulation is augmented with a volumetric integral that includes derivatives of test and trial functions along the quasi-normal directions to $\Gamma_h(t_n)$. The integral is computed over tetrahedra cut by the surface at the given time t_n and possibly (depending on the surface normal velocity and the time step size) over a few more layers of the tetrahedra. The benefit of the augmentation is threefold: first, it implicitly defines an extension of the solution to a narrow band of the surface hence eliminating the need for FMM or any other additional modulus; second, it stabilizes the method algebraically leading to well-conditioned matrices; finally, it leads to a concise variational formulation of the method and so allows numerical stability and error analysis. The paper presents such analysis as well as the analysis of algebraic stability for the fully discrete method (no simplified assumptions are made such as numerical integration over exact surface). The analysis allows background finite element spaces of arbitrary order $m \geq 1$. We notice however that for $m > 1$ and optimal order convergence, numerical integration with higher order accuracy is required which is a non-trivial task; cf. remark 4.1 below. For the time discretization we apply the backward Euler method. Higher order in time discretizations are straightforward, and we illustrated them in numerical example section, but they are not covered by the presented analysis.

The remainder of the paper is organized as follows. In section 2 we review the surface transport–diffusion equation as an example of a PDE posed on an evolving surface. To elucidate the main ideas behind the method and analysis, section 3 introduces a semi-discrete method (FD in time / continuous in space) and presents its stability analysis. Further, in section 4 we devise a fully discrete method. In section 5 the core analysis of the paper is given. The section opens with several important preparatory results, then proceeds to the stability analysis of the fully discrete method and closes up with the error analysis in the energy norm. For the error analysis, one has to handle approximation errors in time and space together with geometric errors resulting from numerical recovery of the surface (we do not assume that any explicit patchwise parametrization of $\Gamma(t)$ is known). In section 6 we prove bounds on condition numbers of resulting matrices, which are independent of how the surface cuts through the background mesh. Results of several numerical experiments, which illustrate the theoretical findings and show optimal convergence order also in weaker norms, are collected in section 7. Section 8 gives some conclusions and discusses interesting open problems.

2. Mathematical problem. Consider a surface $\Gamma(t)$ passively advected by a smooth velocity field $\mathbf{w} = \mathbf{w}(\mathbf{x}, t)$, i.e. the normal velocity of $\Gamma(t)$ is given by $\mathbf{w} \cdot \mathbf{n}$, with $\mathbf{n}$ the unit normal on $\Gamma(t)$. We assume that for all $t \in [0, T]$, $\Gamma(t)$ is a smooth hypersurface that is closed ($\partial \Gamma = \emptyset$), connected, oriented, and contained in a fixed domain $\Omega \subset \mathbb{R}^d$, $d = 2, 3$. In the remainder we consider $d = 3$,

but all results have analogs for the case $d = 2$.

As an example of the surface PDE, consider the transport–diffusion equation modelling the conservation of a scalar quantity u with a diffusive flux on $\Gamma(t)$ (cf. [23]):

$$(1) \qquad \dot{u} + (\mathrm{div}_\Gamma \mathbf{w})u - \nu \Delta_\Gamma u = 0 \quad \text{on} \ \ \Gamma(t), \ \ t \in (0, T],$$

with initial condition $u(\mathbf{x}, 0) = u_0(\mathbf{x})$ for $\mathbf{x} \in \Gamma^0 := \Gamma(0)$. Here $\dot{u}$ denotes the advective material derivative, $\mathrm{div}_\Gamma := \mathrm{tr}\left((I - \mathbf{n}\mathbf{n}^T)\nabla\right)$ is the surface divergence, Δ_Γ is the Laplace–Beltrami operator, and $\nu > 0$ is the constant diffusion coefficient. The well-posedness of suitable weak formulations of (1) has been proven in [9, 36, 1].

The equation (1) can be written in several equivalent forms, see [10]. In particular, for any smooth extension of u from the space–time manifold

$$\mathcal{G} = \bigcup_{t \in (0, T)} \Gamma(t) \times \{t\}, \quad \mathcal{G} \subset \mathbb{R}^4,$$

to a neighborhood of $\mathcal{G}$, one can expand $\dot{u}$ using the Cartesian derivatives

$$\dot{u} = \frac{\partial u}{\partial t} + \mathbf{w} \cdot \nabla u.$$

In this paper, we assume that $\Gamma(t)$ is the zero-level set of a smooth level-set function $\phi(\mathbf{x}, t)$,

$$\Gamma(t) = \{\mathbf{x} \in \mathbb{R}^3 \ : \ \phi(t, \mathbf{x}) = 0\},$$

such that $|\nabla \phi| \geq c > 0$ in $\mathcal{O}(G)$, a neighborhood of $\mathcal{G}$. Note that we do not assume that ϕ is a signed distance function. The method that we introduce can deal with more general level set functions. However, the analysis (sections 3.3, 4 and 5) uses the assumption of a level set function with the signed distance property in order to keep the amount of technical details at a comprehensive level, cf. the introductory part of section 3.3.

For a smooth u defined on $\mathcal{G}$, a function u^e denotes the extension of u to $\mathcal{O}(G)$ along spatial normal directions to the level-sets of ϕ, it holds $\nabla u^e \cdot \nabla \phi = 0$ in $\mathcal{O}(G)$, $u^e = u$ on $\mathcal{G}$. The extension u^e is smooth once ϕ and u are both smooth. Further, we use the same notation u for the function on $\mathcal{G}$ and its extension to $\mathcal{O}(G)$. We shall write $\mathcal{O}(\Gamma(t))$ to denote a neighborhood of $\Gamma(t)$ in $\mathbb{R}^3$, which is the time cross-section of $\mathcal{G}$, $\mathcal{O}(\Gamma(t)) := \{\mathbf{x} \in \mathbb{R}^3 \ : \ (t, \mathbf{x}) \in \mathcal{O}(G)\}$.

We can rewrite (1) as follows:

$$(2) \qquad \begin{cases} \frac{\partial u}{\partial t} + \mathbf{w} \cdot \nabla u + (\mathrm{div}_\Gamma \mathbf{w})u - \nu \Delta_\Gamma u = 0 & \text{on} \ \ \Gamma(t), \\ \nabla u \cdot \nabla \phi = 0 & \text{in} \ \ \mathcal{O}(\Gamma(t)) \end{cases} \quad t \in (0, T].$$

This formulation will be used for the discretization method.

3. Discretization in time.

3.1. Preliminaries and notation. We introduce notation for the surfaces at discrete time levels. For simplicity of notation, consider the uniform time step $\Delta t = T/N$, and let $t_n = n\Delta t$ and $I_n = [t_{n-1}, t_n)$. Denote by u^n an approximation of $u(t_n)$, define $\Gamma^n := \Gamma(t_n)$ and $\phi^n(\mathbf{x}) := \phi(\mathbf{x}, t_n)$, $n = 0, \dots, N$. We assume that $\mathcal{O}(G)$ is a sufficiently large neighborhood of $\mathcal{G}$ such that

$$(3) \qquad \Gamma^n \subset \mathcal{O}(\Gamma^{n-1}) \quad \text{for } n = 1, \dots, N, \text{ cf. Fig. 1}.$$

In this case, u^{n-1} is well-defined on Γ^n. Further, we use the following abbreviations in norms and scalar products for functions u, v in a domain G: $(u, v)_G := (u, v)_{L^2(G)}$, $\|u\|_G := \|u\|_{L^2(G)}$, $\|u\|_{\infty,G} := \|u\|_{L^\infty(G)}$. We also introduce the decomposition $\mathbf{w} = \mathbf{w}_T + w_N \mathbf{n}$ where $\mathbf{w}_T$ and $w_N \mathbf{n}$ denote the tangential and normal parts of the velocity vector field $\mathbf{w}$ on $\Gamma(t)$. Further, for a function v defined on $\Gamma(t)$ or on $\mathcal{O}(\Gamma(t))$ we introduce several abbreviated maximum norms at time levels, intervals and the whole time domain:

$$(4\mathrm{a}) \quad \|v\|_{\infty,n} := \|v\|_{\infty,\Gamma^n}, \qquad \|v\|_{\infty,I_n} := \sup_{t \in I_n} \|v\|_{\infty,\Gamma(t)}, \qquad \|v\|_\infty := \sup_{t \in [0,T]} \|v\|_{\infty,\Gamma(t)},$$

$$(4\mathrm{b}) \quad \|v\|_{\infty,n,\mathcal{O}} := \|v\|_{\infty,\mathcal{O}(\Gamma^n)}, \quad \|v\|_{\infty,I_n,\mathcal{O}} := \sup_{t \in I_n} \|v\|_{\infty,\mathcal{O}(\Gamma(t))}, \quad \|v\|_{\infty,\mathcal{O}} := \sup_{t \in [0,T]} \|v\|_{\infty,\mathcal{O}(\Gamma(t))}.$$

Γ^{n-1}

$\Gamma^n \subset \mathcal{O}(\Gamma^{n-1})$
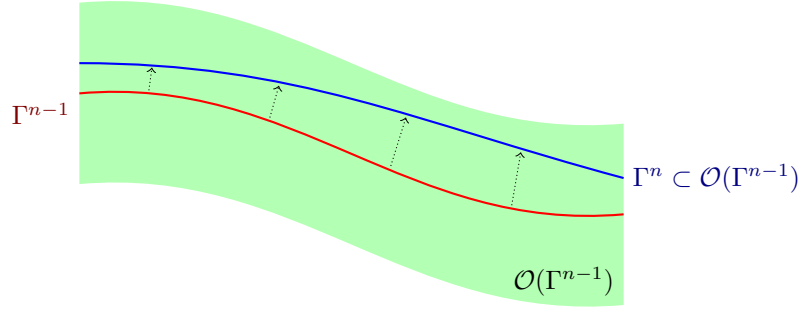
$\mathcal{O}(\Gamma^{n-1})$

FIG. 1. *Sketch of interface positions at different time instances and the neighborhood of one of these interfaces.*

3.2. Time discretization method. The implicit Euler method for (2) is

(5)
$$\begin{cases} \dfrac{u^n - u^{n-1}}{\Delta t} + \mathbf{w}^n \cdot \nabla u^n + (\operatorname{div}_\Gamma \mathbf{w}^n)u^n - \nu \Delta_\Gamma u^n = 0, & \text{on } \Gamma^n, \\ \\ \nabla u^n \cdot \nabla \phi^n = 0, & \text{in } \mathcal{O}(\Gamma^n). \end{cases}$$

Obvious modifications are required to devise higher order time discretizations. For example, for the $O(\Delta t^2)$ method one can use BDF2 approximation of the time derivative, replacing $\frac{u^n - u^{n-1}}{\Delta t}$ by $\frac{3u^n - 4u^{n-1} + u^{n-2}}{2\Delta t}$ in (5) and additionally assuming $\Gamma^n \subset \mathcal{O}(\Gamma^{n-2})$, cf. also Remark 5.2.

Variational formulation in space. The basis for the spatial discretization is a variational formulation in space. For every time instance t we denote by $\mathcal{V}(t)$ the Hilbert space of functions which are defined in a neighborhood of $\Gamma(t)$ and are constant in the direction of the gradient of ϕ (the normal direction), $\mathcal{V}(t) := \overline{\mathcal{V}_*(t)}^{\|\cdot\|_\mathcal{V}}$ with

$$\mathcal{V}_*(t) = \{v \in C^1(\mathcal{O}(\Gamma(t))) \mid \nabla v \cdot \nabla \phi = 0\} \text{ and } \|v\|_\mathcal{V} := \left(\|v\|_{H^1(\Gamma(t))}^2 + \|\nabla \phi \cdot \nabla v\|_{L^2(\mathcal{O}(\Gamma(t)))}^2 \right)^{\frac{1}{2}}.$$

Note that on $\mathcal{V}(t)$ there holds $\|\cdot\|_{H^1(\Gamma(t))} = \|\cdot\|_\mathcal{V}$ and thus $\|\cdot\|_{H^1(\Gamma(t))}$ is a norm. Assume $u^{n-1} \in L^2(\Gamma^{n-1})$ is given, with $u^{n-1} \in \mathcal{V}(t_{n-1})$ and (3). We seek for $u^n \in \mathcal{V}(t_n)$ such that for all $v \in \mathcal{V}(t_n)$ there holds

(6)
$$\int_{\Gamma^n} \left(\frac{1}{\Delta t} u^n + \mathbf{w} \cdot \nabla u^n + (\operatorname{div}_\Gamma \mathbf{w})u^n \right) v \, ds + \nu \int_{\Gamma^n} \nabla_\Gamma u^n \cdot \nabla_\Gamma v \, ds = \int_{\Gamma^n} \frac{1}{\Delta t} u^{n-1} v \, ds.$$

Note that the second equation of (5) is hidden in the definition of space $\mathcal{V}(t_n)$ in (6). Below, in the finite element method we will impose it weakly through the variational formulation.

Integration by parts characterization of the convection term. Since $\Gamma(t)$ is smooth and closed, we have the integration by parts identity:

$$\int_{\Gamma(t)} (\mathbf{w} \cdot \nabla u)v \, ds = \int_{\Gamma(t)} (\mathbf{w}_T \cdot \nabla_\Gamma u)v \, ds = -\int_{\Gamma(t)} (\mathbf{w}_T \cdot \nabla_\Gamma v + (\operatorname{div}_\Gamma \mathbf{w}_T)v)u \, ds$$
$$= \frac{1}{2} \int_{\Gamma(t)} (\mathbf{w}_T \cdot \nabla_\Gamma uv - \mathbf{w}_T \cdot \nabla_\Gamma vu) \, ds - \frac{1}{2} \int_{\Gamma(t)} (\operatorname{div}_\Gamma \mathbf{w}_T)uv \, ds$$

for $u, v \in \mathcal{V}(t)$. Note that we exploited $\mathbf{n} = \nabla \phi / |\nabla \phi|$ on $\Gamma(t)$ and so $\mathbf{n} \cdot \nabla u = \mathbf{n} \cdot \nabla v = 0$ here. We will use the integration by part characterization (7) in our analysis and also to define the finite element method.

Unique solvability. To guarantee unique solvability in every time step, we ask for coercivity of the left-hand side bilinear form in (6) with respect to $\|\cdot\|_{H^1(\Gamma^n)}$. Testing (6) with $v = u^n$ and exploiting (7) clarifies that a sufficient condition for coercivity is

(7)
$$\Delta t \le (2\xi)^{-1} \text{ with } \xi := \|\operatorname{div}_\Gamma(\mathbf{w} - \frac{1}{2}\mathbf{w}_T)\|_\infty.$$

4

Using the notation $\kappa(t) = \operatorname{div}_\Gamma \mathbf{n}_\Gamma$ for the mean curvature, we have $\operatorname{div}_\Gamma \mathbf{w} = \operatorname{div}_\Gamma \mathbf{w}_T + \kappa(t) w_N$ and can also express condition (7) with

$$\xi = \|\frac{1}{2} \operatorname{div}_\Gamma \mathbf{w}_T + \kappa(t) w_N\|_\infty.$$

3.3. Stability of the semi-discrete method. We now show a numerical stability bound for u^n. The goal of this paper is the study of a fully discrete method, but the treatment of the semi-discrete problem (5) gives some insight and serves for the purpose of better exposition. From now on we *assume that ϕ is the signed distance function* for $\Gamma(t)$ in $\mathcal{O}(\Gamma(t))$ for $t \in [0, T]$. Although this assumption is not essential, it simplifies our further (still rather technical) analysis. We assume $\Gamma(t)$ and its evolution are smooth such that $\phi \in C^2(\mathcal{O}(\mathcal{G}))$

Denote by $\mathbf{p}(\mathbf{x}, t) : \mathcal{O}(\Gamma(t)) \to \Gamma(t)$ the closest point projection on $\Gamma(t)$. Then using that ϕ is the signed distance function the second equation in (5) can be written as $u^n(\mathbf{x}) = u^n(\mathbf{p}^n(\mathbf{x}))$ in $\mathcal{O}(\Gamma^n)$, $\mathbf{p}^n(\mathbf{x}) = \mathbf{p}(\mathbf{x}, t_n)$; and the passive advection of Γ by the velocity field yields

$$(8) \qquad \frac{\partial \phi}{\partial t} = -w_N \circ \mathbf{p} \quad \text{in } \mathcal{O}(\mathcal{G}).$$

We need the following result.

LEMMA 1. *For $v \in L^2(\Gamma^{n-1})$ the following estimate holds:*

$$(9) \qquad \|v \circ \mathbf{p}^{n-1}\|_{\Gamma^n}^2 \leq (1 + c_1 \Delta t) \|v\|_{\Gamma^{n-1}}^2 \quad \text{with} \quad c_1 = c(\|w_N\|_{\infty, I_n} + \Delta t \|\nabla_\Gamma w_N\|_{\infty, I_n})$$

and a constant c independent of Δt, n, v.

Proof. For $\mathbf{y} \in \Gamma^{n-1}$ denote by $\kappa_i(\mathbf{y})$, $i = 1, 2$, two principle curvatures, and let

$$(10) \qquad \kappa_i(\mathbf{x}) = \kappa_i(\mathbf{p}^{n-1}(\mathbf{x})) \left[1 + \phi^{n-1}(\mathbf{x})\kappa_i(\mathbf{p}^{n-1}(\mathbf{x}))\right]^{-1} \quad \mathbf{x} \in \mathcal{O}(\Gamma^{n-1}).$$

The surface measures on Γ^{n-1} and Γ^n satisfy, see, e.g., [7, Proposition 2.1],

$$\mu^n(\mathbf{x}) d\mathbf{s}^n(\mathbf{x}) = d\mathbf{s}^{n-1}(\mathbf{p}^{n-1}(\mathbf{x})), \quad \mathbf{x} \in \Gamma^n, \quad \text{with}$$
$$(11) \qquad \mu^n(\mathbf{x}) = \underbrace{(1 - \phi^{n-1}(\mathbf{x})\kappa_1(\mathbf{x}))}_{=:a_1} \underbrace{(1 - \phi^{n-1}(\mathbf{x})\kappa_2(\mathbf{x}))}_{=:a_2} \underbrace{\nabla\phi^n(\mathbf{x})^T \nabla\phi^{n-1}(\mathbf{x})}_{=:b}.$$

We want to bound $|\mu^n(\mathbf{x}) - 1|$. There is a constant $c > 1$, satisfying $c^{-1} \leq a_1, a_2, b \leq c$, such that we can split the estimate as follows:

$$(12) \quad |\mu^n(\mathbf{x}) - 1| \leq |a_1 a_2 b - 1| \leq |a_1 - 1| a_2 b + |a_2 - 1| b + |b - 1| \leq c(|a_1 - 1| + |a_2 - 1| + |b - 1|).$$

We start with $|a_i - 1| = |\phi^{n-1}(\mathbf{x})||\kappa_i(\mathbf{x})|$, $i = 1, 2$. Using $\phi^n(\mathbf{x}) = 0$ for $\mathbf{x} \in \Gamma^n$ and (8), we get

$$(13) \qquad |\phi^{n-1}(\mathbf{x})| = |\phi^{n-1}(\mathbf{x}) - \phi^n(\mathbf{x})| \leq \|w_N\|_{\infty, I_n} \Delta t.$$

Using the smoothness of ϕ and (8), we also get with $w_N^e := w_N \circ \mathbf{p}$

$$(14) \qquad |1 - b| = |1 - \nabla\phi^n(\mathbf{x})^T \nabla\phi^{n-1}(\mathbf{x})| = \frac{1}{2}|\nabla\phi^n(\mathbf{x}) - \nabla\phi^{n-1}(\mathbf{x})|^2 \leq \frac{1}{2}\|\nabla w_N^e\|_{\infty, I_n, \mathcal{O}}^2 |\Delta t|^2.$$

We further note the identity, see, e.g., [7, (2.2.16)],

$$\nabla w_N^e(\mathbf{x}) = \left(\mathbf{I} - \phi^{n-1}(\mathbf{x})\nabla^2\phi^{n-1}(\mathbf{x})\right) \nabla_\Gamma w_N(\mathbf{p}^{n-1}(\mathbf{x})).$$

From this and (14) we conclude

$$(15) \qquad |1 - b| \leq \frac{1}{2} c \, \|\nabla_\Gamma w_N\|_{\infty, I_n}^2 |\Delta t|^2,$$

with a constant c that depends only on the curvatures of Γ. Now (11), (13) and (15) imply

$$(16) \qquad |1 - \mu^n(\mathbf{x})| \leq c_1 \Delta t, \quad \text{for } \mathbf{x} \in \Gamma^n,$$

and so (9) holds. $\qquad\qquad\qquad\qquad\qquad\qquad\qquad\qquad\qquad\qquad\qquad\qquad\qquad\qquad\qquad\qquad\quad\square$

5

In the next lemma we show *numerical stability* of the semi-discrete scheme.

LEMMA 2. *For $\{u^k\}_{k=1,\dots,N}$ the solution of (6) with initial data $u^0 \in L^2(\Gamma^0)$ there holds*

$$(17) \qquad \|u^k\|_{\Gamma^k}^2 + 2\Delta t\nu \sum_{n=1}^{k} \|\nabla_\Gamma u^n\|_{\Gamma^n}^2 \leq \exp(c_2 t_k)\|u^0\|_{\Gamma^0}^2, \quad \text{for } k = 0, \dots, N,$$

for a constant c_2 that is independent of Δt and k.

Proof. We test (6) with $2u^n$ and apply (7) to get

$$\|u^n\|_{\Gamma^n}^2 + \|u^n - u^{n-1}\|_{\Gamma^n}^2 + 2\Delta t\nu\|\nabla_\Gamma u^n\|_{\Gamma^n}^2 + 2\Delta t(\operatorname{div}_\Gamma(\mathbf{w} - \frac{1}{2}\mathbf{w}_T)u^n, u^n)_{\Gamma^n} = \|u^{n-1}\|_{\Gamma^n}^2.$$

Now we recall that the second equation in (5) implies $u^{n-1}(\mathbf{x}) = u^{n-1}(\mathbf{p}^{n-1}(\mathbf{x}))$ on Γ^n and we use (9) for the right-hand side term; we also estimate the divergence term using the definition of ξ in (7). This gives

$$(18) \qquad (1 - 2\xi\Delta t)\|u^n\|_{\Gamma^n}^2 + 2\Delta t\nu\|\nabla_\Gamma u^n\|_{\Gamma^n}^2 \leq (1 + c_1\Delta t)\|u^{n-1}\|_{\Gamma^{n-1}}^2$$

We sum up these inequalities for $n = 1, \dots, k$, $k \leq N$, and get

$$\alpha\|u^k\|_{\Gamma^k}^2 + 2\Delta t\nu \sum_{n=1}^{k} \|\nabla_\Gamma u^n\|_{\Gamma^n}^2 \leq \|u^0\|_{\Gamma^0}^2 + (c_1 + 2\xi)\Delta t \sum_{n=0}^{k-1} \|u^n\|_{\Gamma^n}^2, \quad \text{with } \alpha = 1 - 2\xi\Delta t > 0.$$

The quantities c and ξ depend only on the PDE problem data such as $\mathbf{w}$ and Γ, but not on numerical parameter Δt. In particular, one can always assume Δt sufficiently small such that $\alpha > \frac{1}{2}$. Applying discrete Gronwall's inequality leads to the stability estimate (17). $\qquad\square$

REMARK 3.1. The stability estimate (17) admits exponential growth. This is rather natural, since the divergence term in (1) is not sign definite and the concentration u may grow exponentially if the (local) area of $\Gamma(t)$ shrinks when the surface evolves; see, e.g., analysis and a priori estimates in [36]. The exponential growth does not happen if the divergence term is non-negative or if the tangential diffusion of u is strong enough to suppress such growth; cf. Proposition 4.5 in [36]. Stability analysis may account for this phenomena by invoking conservation of total mass principle and the Friedrichs inequality,

$$\int_{\Gamma(t)} |\nabla_\Gamma u|^2 \, ds \geq c_F(t) \int_{\Gamma(t)} (u - \frac{1}{|\Gamma(t)|}\bar{u})^2 \, ds \quad \text{for all } t \in [0, T],$$

with $c_F(t) > 0$ and $\bar{u}(t) := \int_{\Gamma(t)} u(s, t) \, ds$. If no additional care is taken, the numerical method (5) conserves mass only approximately. One way to ensure total mass conservation for the numerical solution is to introduce a Lagrange multiplier from $\mathbb{R}$ and to add the constraint $\bar{u}^n - \bar{u}^0 = 0$ to the system (5). The alternative is to augment the left-hand side of (5) with the penalty term $\sigma(\bar{u}^n - \bar{u}^0)\bar{v}$, with an augmentation parameter $\sigma \geq 0$, as was done in [33] for the analysis of the space–time method. The stabilizing term improves the mass conservation property and helps to make use of the Friedrichs inequality in the stability estimate. We skip the arguments here, which largely repeat the analysis above and the one in [33]. These arguments bring one to the numerical stability estimate,

$$\|u^k\|_{\Gamma^k}^2 + \frac{1}{2}\Delta t\nu \sum_{n=1}^{k} \|\nabla_\Gamma u^n\|_{\Gamma^n}^2 \leq \|u^0\|_{\Gamma^0}^2 + \frac{1}{2}\Delta t\nu\|\nabla_\Gamma u^0\|_{\Gamma^0}^2 + t_k\sigma|\bar{u}^0|^2, \quad \text{for } k = 0, \dots, N.$$

Now we turn to the fully discrete case. Besides standard technical difficulties of passing from differential equations to algebraic and finite element functional spaces, we need to handle the situation, when the smooth surface Γ^n is approximated by a set of piecewise smooth Γ_h^n, $n = 0, \dots, N$.

4. Discretization in space and time. In order to reduce the repeated use of generic but unspecified constants, further in the paper we write $x \lesssim y$ to state that the inequality $x \leq cy$ holds for quantities x, y with a constant c, which is independent of the mesh parameters h, Δt, time instance t_n, and the position of Γ over the background mesh. Similar we give sense to $x \gtrsim y$; and $x \simeq y$ will mean that both $x \lesssim y$ and $x \gtrsim y$ hold. However, we shall continue to monitor the explicit dependence of the estimate on the (norms of) normal surface velocity w_N.

4.1. Fully discrete method. Assume a family of consistent subdivisions of Ω into shape regular tetrahedra. This constitutes our background time-independent triangulations $\{\mathcal{T}_h\}_{h>0}$, with $\max_{T \in \mathcal{T}_h} \mathrm{diam}(T) \leq h$. V_h denotes the bulk time-independent finite element space,

$$(19) \qquad V_h := \{v_h \in C(\Omega) : v_h|_S \in P_m(S), \forall S \in \mathcal{T}_h\}, \quad m \geq 1.$$

Let ϕ_h be a given continuous piecewise polynomial approximation (with respect to $\mathcal{T}_h$) of the level set function ϕ for all $t \in [0, T]$, which satisfies

$$(20) \qquad \|\phi - \phi_h\|_{\infty,\Omega} + h\|\nabla(\phi - \phi_h)\|_{\infty,\Omega} \lesssim h^{q+1}, \quad \forall\, t \in [0, T],$$

with some $q \geq 1$. For this estimate to hold, we assume that the level set function ϕ has the smoothness property $\phi \in C^{q+1}(\Omega)$. Moreover, we assume that ϕ_h is sufficiently regular in time, s.t. with $\phi_h^n(\mathbf{x}) = \phi_h(\mathbf{x}, t_n)$, $n = 0, \ldots, N$ there holds

$$(21a) \qquad \|\phi_h^{n-1} - \phi_h^n\|_{\infty,\Omega} \lesssim \Delta t \|w_N\|_{\infty,I_n},$$

$$(21b) \qquad \|\nabla\phi_h^{n-1} - \nabla\phi_h^n\|_{\infty,\Omega} \lesssim \Delta t \left(\|w_N\|_{\infty,I_n} + \|\nabla w_N\|_{\infty,I_n}\right), \text{ for } n = 1, \ldots, N.$$

We define the discrete surfaces Γ_h^n approximating Γ^n as the zero level of ϕ_h^n,

$$\Gamma_h^n := \{\mathbf{x} \in \mathbb{R}^3 : \phi_h^n(\mathbf{x}) = 0\}.$$

Γ_h^n is an approximation to Γ^n with

$$(22) \qquad \mathrm{dist}(\Gamma_h^n, \Gamma^n) = \max_{x \in \Gamma_h^n} |\phi^n(\mathbf{x})| = \max_{x \in \Gamma_h^n} |\phi^n(\mathbf{x}) - \phi_h^n(\mathbf{x})| \leq \|\phi^n - \phi_h^n\|_{\infty,\Omega} \lesssim h^{q+1}.$$

Furthermore, $\mathbf{n}_h^n = \nabla\phi_h^n/|\nabla\phi_h^n|$ the normal vector to Γ_h^n and $\mathbf{n}^n = \nabla\phi^n$ the extended normal vector to Γ^n satisfy for $\mathbf{x} \in \Gamma_h^n$

$$|\mathbf{n}_h^n(\mathbf{x}) - \mathbf{n}^n(\mathbf{x})| = \left|\frac{\nabla\phi_h^n(\mathbf{x})}{|\nabla\phi_h^n(\mathbf{x})|} - \nabla\phi^n(\mathbf{x})\right| \leq \underbrace{\frac{1}{|\nabla\phi_h^n(\mathbf{x})|}}_{\leq c}\left|\nabla\phi_h^n(\mathbf{x}) - \nabla\phi^n(\mathbf{x})|\nabla\phi_h^n(\mathbf{x})|\right|$$

$$(23) \qquad \leq c|\nabla\phi_h^n(\mathbf{x}) - \nabla\phi^n(\mathbf{x})| + \underbrace{|\nabla\phi^n(\mathbf{x})|}_{=1} \cdot \left|\underbrace{1}_{\frac{1}{|\nabla\phi|}} - |\nabla\phi_h^n(\mathbf{x})|\right|$$

$$\leq c|\nabla\phi_h^n(\mathbf{x}) - \nabla\phi^n(\mathbf{x})| \lesssim h^q$$

In the following we assume that integrals on Γ_h^n can be computed accurately. In practice, this is only straightforward for piecewise linear ϕ_h^n, i.e. $q = 1$, while for higher order ϕ_h^n more care is needed, cf. Remark 4.1 below.

The numerical method provides an extension of a finite element solution to a narrow band around Γ_h^n, which is defined as the union of tetrahedra from

$$\mathcal{S}(\Gamma_h^n) := \{S \in \mathcal{T}_h : |\phi_h(\mathbf{x})| \leq \delta_n \text{ for some } \mathbf{x} \in S\}, \quad \mathcal{O}(\Gamma_h^n) = \mathrm{int}\left(\bigcup_{S \in \mathcal{S}(\Gamma_h^n)} \overline{S}\right),$$

where

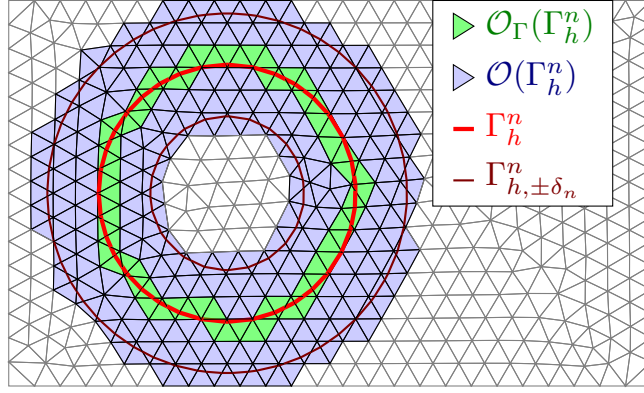$$(24) \qquad \delta_n := c_\delta \|w_N\|_{\infty,I_n} \Delta t$$

7

FIG. 2. *Sketch of discrete domains and interfaces.*

is the minimum thickness of the extension layer and $c_\delta \geq 1$ is an $\mathcal{O}(1)$ mesh-independent constant. Recall that ϕ_h is an approximate distance function, so that $|\phi_h^n| \leq \delta_n$ describes a discrete tubular neighborhood to Γ_h^n. We refer to Figure 2 for a sketch.

In the analysis below, we make use of lifting operators from exact to discrete surfaces. For $n = 1, \ldots, N$ and $k = n-1, 1$ we define the lift operator from Γ^n to Γ_h^k,

(25)
$$\mathbf{l}^{n,k} : \Gamma^n \to \Gamma_h^k, \quad \mathbf{l}^{n,k}(\mathbf{x}) = \mathbf{x} + d^n(\mathbf{x})\mathbf{n}^n(\mathbf{x}),$$

where $d^n(\mathbf{x}) \in \mathbb{R}$ is the smallest (in absolute value) value so that $\mathbf{x} + d^n(\mathbf{x})\mathbf{n}^n(\mathbf{x}) \in \Gamma_h^k$. For $k = n$ we also write $\mathbf{l}^n = \mathbf{l}^{n,n}$. To ensure that these liftings are well-defined bijection mappings we assume that h is sufficiently small. Further, we require that $\delta_n \leq c$ for a constant c that only depends on the temporal resolution of the surface dynamics and the roughness of the surface. We assumed that the surface is smooth at all time so that $\|\kappa\|_{\infty, I_n} \lesssim 1$. Hence, we formulate the following condition on the time step size:

(26)
$$\Delta t \leq c_1 (c_\delta \|w_N\|_{\infty, I_n})^{-1}, \ n = 1, \ldots, N,$$

so that $\delta_n \|\kappa\|_{\infty, I_n} \lesssim \delta_n \lesssim 1$ and the lifting $\mathbf{l}^{n,n-1}$ is well-defined for sufficiently small c_1.

We also denote by $\mathcal{T}_\Gamma^n$ the set of elements intersected by Γ_h^n,

$$\mathcal{T}_\Gamma^n := \{S \in \mathcal{T}_h \ : \ \mathcal{H}_2(S \cap \Gamma_h^n) > 0\} \quad \text{and} \quad \mathcal{O}_\Gamma(\Gamma_h^n) := \text{int}\left(\bigcup_{S \in \mathcal{T}_\Gamma^n} \overline{S}\right).$$

We assume that $\mathcal{O}(\Gamma^n)$ is such that

(27)
$$\mathcal{O}(\Gamma_h^n) \subset \mathcal{O}(\Gamma^n) \quad \text{and} \quad \mathcal{O}_\Gamma(\Gamma_h^{n+1}) \subset \mathcal{O}(\Gamma^n).$$

Note that (20), (21a) and (24) ensure that

(28)
$$c_\delta \text{ sufficiently large implies } \Gamma_h^n \subset \mathcal{O}_\Gamma(\Gamma_h^n) \subset \mathcal{O}(\Gamma_h^{n-1}).$$

This condition is the discrete analog of (3) and it is essential for the well-posedness of the method. We define finite element spaces

(29)
$$V_h^n = \{v \in C(\mathcal{O}(\Gamma_h^n)) \ : \ v \in P_m(S), \forall S \in \mathcal{S}(\Gamma_h^n)\}, \quad m \geq 1.$$

These spaces are the restrictions of the time-independent bulk space V_h on all tetrahedra from $\mathcal{S}(\Gamma_h^n)$.

The numerical method is based on the semi-discrete formulation (6) and identity (7). It reads: For a given $u_h^0 \in V_h^0$ find $u_h^n \in V_h^n$, $n = 1, \ldots, N$, satisfying

(30)
$$\int_{\Gamma_h^n} \left\{ \frac{u_h^n - u_h^{n-1}}{\Delta t} v_h + \frac{1}{2}(\mathbf{w}_T^e \cdot \nabla_{\Gamma_h} u_h^n v_h - \mathbf{w}_T^e \cdot \nabla_{\Gamma_h} v_h u_h^n) + \text{div}_{\Gamma_h}(\mathbf{w}^e - \frac{1}{2}\mathbf{w}_T^e)u_h^n v_h \right\} ds_h$$

$$+ \nu \int_{\Gamma_h^n} \nabla_{\Gamma_h} u_h^n \cdot \nabla_{\Gamma_h} v_h \, ds_h + \rho_n \int_{\mathcal{O}(\Gamma_h^n)} (\mathbf{n}_h \cdot \nabla u_h^n)(\mathbf{n}_h \cdot \nabla v_h) d\mathbf{x} = 0,$$

8

for all $v_h \in V_h^n$. Here $\mathbf{n}_h = \nabla\phi_h/|\nabla\phi_h|$ in $\mathcal{O}(\Gamma_h^n)$, $\rho_n > 0$ is a parameter, $\mathbf{w}^e(\mathbf{x}) = \mathbf{w}(\mathbf{p}^n(\mathbf{x}))$ is lifted data on Γ_h^n from Γ^n. The first term in (30) is well-defined thanks to condition (28). As we discussed in the introduction, the term $\rho_n \int_{\mathcal{O}(\Gamma_h^n)} (\mathbf{n}_h \cdot \nabla u_h^n)(\mathbf{n}_h \cdot \nabla v_h)d\mathbf{x}$ plays several roles. We shall see that for ρ_n not too small, it ensures the form on the left hand side to be elliptic on V_h^n, rather than only on the space of traces. Therefore, on each time step we obtain a FE solution defined in $\mathcal{O}(\Gamma_h^n)$ (this can be seen as an implicit extension procedure). Furthermore, it stabilizes the problem algebraically, i.e. the resulting systems of algebraic equations are well-conditioned in a suitable sense, see section 6.

REMARK 4.1 (Numerical integration). The discrete surface Γ_h^n is described only implicitly via the zero-level of a discrete level set function. In general, it is a non-trivial task to obtain a parametrized representation of Γ_h^n which would allow for a straightforward application of numerical quadrature rules. On simplices and in the low order case where ϕ_h is a piecewise linear approximation of the level set function ϕ ($q = 1$ in (20)), an explicit reconstruction of Γ_h^n is easily available, cf. e.g. [29]. On hyperrectangles, a low order case where the accuracy of the implicit representation is $q = 1$ in (20) can be dealt with a marching cube [27] approximation. However, the higher order case $q > 1$ is more involved and requires special approaches for the construction of quadrature rules. We do not extend this discussion here but refer to the literature instead, cf. [14, 25, 31, 38, 41, 43].

5. Analysis of the fully discrete method. In this section we carry out the numerical analysis of the fully discrete method. Before we can perform the stability and consistency analysis (subsections 5.3 and 5.4) to derive a priori error bounds in subsection 5.5, we require two results that are technically more involved. The first one gives control in the L^2 norm in a narrow band volume based on a combination of the L^2 norm on the surface and the normal gradient in the volume that is provided by the stabilization. The result is treated in subsection 5.1 and is a generalization of a result from [4] which is also found in [16, Lemma 7.6]. The second result provides bounds for the evaluation of a lifting of a function that is naturally defined on Γ_h^{n-1} to Γ_h^n. The result is the counterpart to Lemma 1 on the discrete level and is treated in subsection 5.2.

5.1. Volume control by the normal diffusion stabilization. Before we can state and prove the lemma on the normal diffusion stabilization we need some preparation.

We denote the limiting level sets of ϕ_h with $|\phi_h| = \delta_n$ as $\Gamma_{h,\pm\delta_n}^n := \{\phi_h(\mathbf{x}) = \pm\delta_n\}$. The corresponding set of elements cut by $\Gamma_{h,\pm\delta_n}^n$ is denoted by $\mathcal{O}_\Gamma(\Gamma_{h,\pm\delta_n}^n)$, cf. Figure 2. Now, we introduce a mapping $\Phi : \mathcal{O}(\Gamma_h^n) \to \mathcal{O}(\Gamma^n)$ that allows to map from approximated level sets to exact level sets. For $\mathbf{x} \in \mathcal{O}(\Gamma_h^n)$ we define $\Phi(\mathbf{x}) := \mathbf{x} + (\phi_h^n(\mathbf{x}) - \phi^n(\mathbf{x}))\mathbf{n}(\mathbf{x})$ with $\mathbf{n}(\mathbf{x}) = \nabla\phi(\mathbf{x}) = \mathbf{n}(\mathbf{p}^n(\mathbf{x}))$ which has $\phi^n \circ \Phi = \phi_h^n$ in $\mathcal{O}(\Gamma_h^n)$, i.e.

$$(31) \qquad \phi^n(\mathbf{x} + (\phi_h^n(\mathbf{x}) - \phi^n(\mathbf{x}))\mathbf{n}(\mathbf{x})) = \phi^n(\mathbf{x}) + \phi_h^n(\mathbf{x}) - \phi^n(\mathbf{x}) = \phi_h^n(\mathbf{x}) \quad \forall \, \mathbf{x} \in \mathcal{O}(\Gamma_h^n).$$

LEMMA 3. *The mapping Φ is well-defined, continuous and $\Phi|_S \in C^{q+1}(S)$ for any $S \in \mathcal{S}(\Gamma_h^n)$. There hold $\Phi(\Gamma_h^n) = \Gamma^n$ and*

$$(32) \qquad \|\Phi - \mathrm{id}\,\|_{\infty,\mathcal{O}(\Gamma_h^n)} \lesssim h^{q+1}, \quad \|D\Phi - I\|_{\infty,\mathcal{O}(\Gamma_h^n)} \lesssim h^q.$$

Further, for h sufficiently small Φ is invertible.

Proof. The smoothness is obtained by construction. To see $\Phi(\Gamma_h^n) = \Gamma^n$ we recall that $\phi^n \circ \Phi = \phi_h^n$ holds also for $\mathbf{x} \in \Gamma_h^n = \{\phi_h^n = 0\}$ which implies that $\Phi(\mathbf{x}) \in \Gamma^n = \{\phi^n = 0\}$. Finally, (32) follows from (20). □

We use this mapping to map from the discrete surface to the exact one. We introduce the following notation. For $u \in V_h^n$ we define $\tilde{u} := u \circ \Phi^{-1}$, $\tilde{\mathcal{O}}(\Gamma_h^n) := \Phi(\mathcal{O}(\Gamma_h^n))$ and $\Gamma_{\pm\delta_n} := \Phi(\Gamma_{h,\pm\delta_n}^n) = \{\phi(\mathbf{x}) = \pm\delta_n\}$. Due to (32) we have that

$$(33) \qquad \|\tilde{u}\|_{\tilde{\mathcal{O}}(\Gamma_h^n)}^2 = \int_{\tilde{\mathcal{O}}(\Gamma_h^n)} \tilde{u}^2 \, d\mathbf{x} = \int_{\mathcal{O}(\Gamma_h^n)} \underbrace{\det(D\Phi)}_{\simeq 1} u^2 \, d\mathbf{x} \simeq \|u\|_{\mathcal{O}(\Gamma_h^n)}^2$$

and similarly one easily shows (see, e.g., [26, Lemma 3.7])

$$(34) \qquad \|u\|_{\Gamma_h^n}^2 \simeq \|\tilde{u}\|_{\Gamma^n}^2.$$

LEMMA 4. *On a quasi-uniform family of triangulations, for sufficiently small h, for* $\tilde{u} \in V_h^n \circ \Phi^{-1}$ *there hold*

$$(35) \qquad \|\tilde{u}\|^2_{\tilde{\mathcal{O}}_\Gamma(\Gamma^n_{h,\pm\delta_n})} \lesssim h\|\tilde{u}\|^2_{\Gamma^n_{\pm\delta_n}} + h^2\|\mathbf{n}\cdot\nabla\tilde{u}\|^2_{\tilde{\mathcal{O}}_\Gamma(\Gamma^n_{h,\pm\delta_n})}.$$

Proof. The technical proof is given in [16, section 7.2]. The main idea is the application of the co-area formula combined with estimates along paths which are normal to the interfaces $\Gamma^n_{\pm\delta_n}$ and cross the interfaces $\Gamma^n_{\pm\delta_n}$. Below in Theorem 5 we apply similar techniques. $\square$

THEOREM 5. *For h sufficiently small and Δt so that (26) is fulfilled, the following uniform with respect to δ_n, h and n estimate holds:*

$$(36) \qquad \|u\|^2_{\mathcal{O}(\Gamma^n_h)} \lesssim (\delta_n + h)\|u\|^2_{\Gamma^n_h} + (\delta_n + h)^2\|\mathbf{n}_h\cdot\nabla u\|^2_{\mathcal{O}(\Gamma^n_h)} \quad \text{for all } u \in V_h^n,$$

with δ_n from (24).

Proof. We start on the mapped domain by an overlapping decomposition of $\tilde{\mathcal{O}}(\Gamma^n_h)$ into $U_{\delta_n}(\Gamma) :=$ ▮ $\{\mathbf{x} \in \mathbb{R}^3 : |\phi^n(\mathbf{x})| < \delta_n\}$ and $\tilde{\mathcal{O}}_\Gamma(\Gamma^n_{h,\pm\delta_n})$ and apply Lemma 4:

$$(37) \qquad \begin{aligned}\|u\|^2_{\mathcal{O}(\Gamma^n_h)} &\simeq \|\tilde{u}\|^2_{\tilde{\mathcal{O}}(\Gamma^n_h)} \leq \|\tilde{u}\|^2_{U_{\delta_n}(\Gamma)} + \|\tilde{u}\|^2_{\tilde{\mathcal{O}}_\Gamma(\Gamma^n_{h,\pm\delta_n})} \\ &\lesssim \|\tilde{u}\|^2_{U_{\delta_n}(\Gamma)} + h\|\tilde{u}\|^2_{\Gamma^n_{\pm\delta_n}} + h^2\|\mathbf{n}\cdot\nabla\tilde{u}\|^2_{\tilde{\mathcal{O}}_\Gamma(\Gamma^n_{h,\pm\delta_n})}.\end{aligned}$$

To treat the integral on U_{δ_n} and $\Gamma^n_{\pm\delta_n}$, we proceed similar to [16, Lemma 7.4] and use the co-area formula, cf. e.g. [10, Theorem 2.9]. To this end we introduce the coordinates $\mathbf{x} = (\xi, s)$ so that $\mathbf{x} = r_\xi(s) = \xi + s\mathbf{n}(\xi)$ and introduce the line $R_\xi := \{r_\xi(s), s \in [-\delta_n, \delta_n]\}$. Then, there holds

$$\int_{U_{\delta_n}} f(\mathbf{x}) \, d\mathbf{x} = \int_{\Gamma^n} \int_{-\delta_n}^{\delta_n} J(\mathbf{x})^{-1} f(\xi + s\mathbf{n}(\xi)) \, ds \, d\xi$$

with the normal-Jacobian J and $J(\mathbf{x})^{-1} = \det(I + s(\mathbf{x})H(\xi))$ where $H = D^2 s$ is the Hessian of $s(\mathbf{x}) = \phi^n(\mathbf{x})$. We have with (26)

$$(38) \qquad J^{-1} = \det(I - s(\mathbf{x})H(\mathbf{x})) \lesssim 1 + \delta_n \underbrace{\text{tr}(H(\mathbf{x}))}_{=\kappa(\xi)} \lesssim 1.$$

Thus, we can estimate the integral over U_{δ_n} in (37) based on iterated integrals. There holds with the Cauchy-Schwarz and Young's inequality

$$(39) \qquad \tilde{u}(\xi, s)^2 = \tilde{u}(\xi, 0)^2 + 2\int_0^s \tilde{u}(\xi, t) \underbrace{\partial_s \tilde{u}(\xi, t)}_{=\mathbf{n}(\xi)\cdot\nabla\tilde{u}(\xi,t)} \, dt \leq \tilde{u}(\xi, 0)^2 + \frac{1}{\gamma}\|\tilde{u}\|^2_{R_\xi} + \gamma\|\mathbf{n}\cdot\nabla\tilde{u}\|^2_{R_\xi}.$$

For the integral over U_{δ_n}, we choose $\gamma = 8\delta_n$ and integrate over $(-\delta_n, \delta_n)$, where we choose $\gamma = 4h$ to estimate $\tilde{u}(\xi, \pm\delta_n)$ which yields

$$\begin{aligned}\|\tilde{u}\|^2_{R_\xi} + h\sum_\pm \tilde{u}(\xi, \pm\delta_n)^2 \leq &2\delta_n\tilde{u}(\xi,0)^2 + \frac{2\delta_n}{8\delta_n}\|\tilde{u}\|^2_{R_\xi} + 16\delta_n^2\|\mathbf{n}\cdot\nabla\tilde{u}\|^2_{R_\xi} \\ &+ 2h\tilde{u}(\xi,0)^2 + \frac{h}{4h}\|\tilde{u}\|^2_{R_\xi} + 4h^2\|\mathbf{n}\cdot\nabla\tilde{u}\|^2_{R_\xi} \\ \leq &4(\delta_n + h)\tilde{u}(\xi,0)^2 + (32\delta_n^2 + 8h^2)\|\mathbf{n}\cdot\nabla\tilde{u}\|^2_{R_\xi}.\end{aligned}$$

and integrating over $\xi \in \Gamma$ gives

$$(40) \qquad \|\tilde{u}\|^2_{U_{\delta_n}(\Gamma)} + h\|\tilde{u}\|^2_{\Gamma^n_{\pm\delta_n}} \lesssim (\delta_n + h)\|\tilde{u}\|^2_\Gamma + (\delta_n + h)^2\|\mathbf{n}\cdot\nabla\tilde{u}\|^2_{U_{\delta_n}(\Gamma)}.$$

Plugging this into (37) we have

$$\|u\|^2_{\mathcal{O}(\Gamma^n_h)} \simeq \|\tilde{u}\|^2_{\tilde{\mathcal{O}}(\Gamma^n_h)} \lesssim (\delta_n + h)\|\tilde{u}\|^2_\Gamma + (\delta_n + h)^2\|\mathbf{n}\cdot\nabla\tilde{u}\|^2_{\tilde{\mathcal{O}}(\Gamma^n_h)}$$

$$(41) \qquad\qquad\qquad\qquad \lesssim (\delta_n + h)\|u\|^2_{\Gamma^n_h} + (\delta_n + h)^2\|\mathbf{n}\cdot\nabla\tilde{u}\|^2_{\tilde{\mathcal{O}}(\Gamma^n_h)}$$
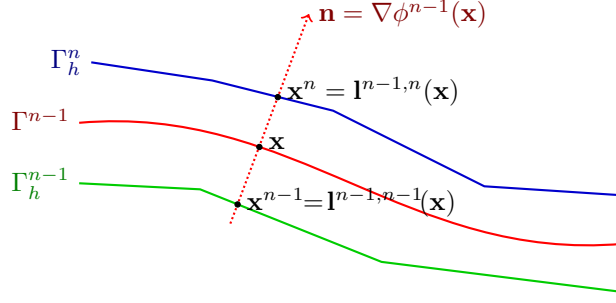
FIG. 3. *Sketch of the geometries in the proof of Lemma 6.*

Finally, we have to bound the normal derivative part on the mapped domain:

$$\|\mathbf{n} \cdot \nabla \tilde{u}\|^2_{\mathcal{O}(\Gamma_h^n)} \lesssim \|\mathbf{n}_h \cdot \nabla u\|^2_{\mathcal{O}(\Gamma_h^n)} + \|D\Phi^{-1} \cdot \mathbf{n} \circ \Phi - \mathbf{n}_h\|^2_{\infty, \mathcal{O}(\Gamma_h^n)} \|\nabla u\|^2_{\mathcal{O}(\Gamma_h^n)}$$

$$(42) \qquad\qquad \overset{(*)}{\lesssim} \|\mathbf{n}_h \cdot \nabla u\|^2_{\mathcal{O}(\Gamma_h^n)} + h^{2q}\|\nabla u\|^2_{\mathcal{O}(\Gamma_h^n)} \lesssim \|\mathbf{n}_h \cdot \nabla u\|^2_{\mathcal{O}(\Gamma_h^n)} + h^{2q-2}\|u\|^2_{\mathcal{O}(\Gamma_h^n)}.$$

Here, we used the following estimate in $(*)$ for $\mathbf{x} \in \mathcal{O}(\Gamma_h^n)$

$$|D\Phi^{-1} \cdot \mathbf{n} \circ \Phi - \mathbf{n}_h| \lesssim \underbrace{|D\Phi^{-1} \cdot \mathbf{n} \circ \Phi - \mathbf{n} \circ \Phi|}_{\lesssim |D\Phi^{-1} - I| \lesssim h^q} + \underbrace{|\mathbf{n} \circ \Phi - \mathbf{n}|}_{\lesssim |\mathbf{n}|_{W^{1,\infty}} |\Phi - \mathrm{id}| \lesssim h^{q+1}} + \underbrace{|\mathbf{n} - \mathbf{n}_h|}_{\lesssim h^q} \lesssim h^q.$$

The final term in (42) can be absorbed by the left hand side due to $c\,h^{2q-2}(\delta_n + h)^2 \le \frac{1}{2}$ for h and Δt sufficiently small which concludes the proof. $\qquad\square$

5.2. Stability of shift operations and the normal diffusion stabilization. To control the effect of the geometric error, we require the following very mild condition in our analysis,

$$(43) \qquad\qquad h^{2q} \le c_h \Delta t,$$

for some c_h independent of Δt and h. We recall that $q \ge 1$ is defined in (20).

Now, we turn our attention to a discrete analogue of Lemma 1 which we prove in two steps.

LEMMA 6. *For $v \in L^2(\Gamma^{n-1})$, Δt so that (26) is fulfilled and the lifting operaros in (25) are well-defined and h so that (43) is fulfilled, it holds*

$$(44) \qquad\qquad \|v \circ \mathbf{p}^{n-1}\|^2_{\Gamma_h^n} \le (1 + c_6 \Delta t) \, \|v \circ \mathbf{p}^{n-1}\|^2_{\Gamma_h^{n-1}}$$

with some c_6 independent of h, Δt, and n.

Proof. For $\mathbf{x} \in \Gamma^{n-1}$, we make use of the lift operators $\mathbf{l}^{n-1,k} : \Gamma^{n-1} \to \Gamma_h^k$, cf. (25) in section 4.1, such that $\mathbf{l}^{n-1,k}(\mathbf{p}^{n-1}(\mathbf{x})) = \mathbf{x}$ on Γ_h^k, $k = n-1, n$. For $\mathbf{x} \in \Gamma^{n-1}$, denote $\mathbf{x}^k = \mathbf{l}^{n-1,k}(\mathbf{x}) \in \Gamma_h^k$, $k = n-1, n$, cf. Figure 3. Similar to (11), the surface measures on Γ_h^k, $k = n-1, n$, satisfy

$$\mu_h^k(\mathbf{x}^k) d\mathbf{s}_h^k(\mathbf{x}^k) = d\mathbf{s}^{n-1}(\mathbf{x}), \quad \mathbf{x} \in \Gamma^{n-1},$$

$$(45) \qquad \mu_h^k(\mathbf{x}^k) = \underbrace{\left(1 - \phi^{n-1}(\mathbf{x}^k)\kappa_1(\mathbf{x}^k)\right)}_{=:a_1^k} \underbrace{\left(1 - \phi^{n-1}(\mathbf{x}^k)\kappa_2(\mathbf{x}^k)\right)}_{=:a_2^k} \underbrace{\mathbf{n}_h^k(\mathbf{x}^k) \cdot \mathbf{n}^{n-1}(\mathbf{x}^k)}_{=:b^k},$$

where we recall (23), $\mathbf{n}_h^k = \nabla \phi_h^k / |\nabla \phi_h^k|$ and set $\mathbf{n}^{n-1} := \nabla \phi^{n-1}$. We need to estimate the term $|1 - \mu_h^n(\mathbf{x}^n)/\mu_h^{n-1}(\mathbf{x}^{n-1})|$ for $\mathbf{x} \in \Gamma^{n-1}$. To this end, we split this term into several parts:

$$|1 - \mu_h^n(\mathbf{x}^n)/\mu_h^{n-1}(\mathbf{x}^{n-1})| = \frac{1}{|\mu_h^{n-1}(\mathbf{x}^{n-1})|}|\mu_h^n(\mathbf{x}^n) - \mu_h^{n-1}(\mathbf{x}^{n-1})| \le c|a_1^n a_2^n b^n - a_1^{n-1} a_2^{n-1} b^{n-1}|$$

$$\le c|(a_1^n - a_1^{n-1})a_2^n b^n + a_1^{n-1}(a_2^n - a_2^{n-1})b^n + a_1^{n-1}a_2^{n-1}(b^n - b^{n-1})|$$

$$(46) \qquad\qquad \le c\left(|a_1^n - a_1^{n-1}| + |a_2^n - a_2^{n-1}| + |b^n - b^{n-1}|\right),$$

11

where we exploited that there is a constant $c > 1$ independent of h, Δt and n so that $c^{-1} \leq a_i^k, b^k \leq c$, $i = 1, 2$, $k = n-1, n$. We start with bounds for $|a_i^n - a_i^{n-1}|$. Since $\phi^{n-1}(\mathbf{x})$ is the signed distance function for Γ^{n-1}, and $\mathbf{l}^{n-1,k}$ is the lift operator along the normal directions to Γ^{n-1}, it holds

$$|\phi^{n-1}(\mathbf{x}^{n-1}) - \phi^{n-1}(\mathbf{x}^n)| = |\mathbf{x}^{n-1} - \mathbf{x}^n|.$$

To estimate the distance on the right-hand side, we note that

$$(\mathbf{x}^{n-1} - \mathbf{x}^n) \cdot \nabla \phi_h^{n-1}(\mathbf{y}) \leq |\phi_h^{n-1}(\mathbf{x}^{n-1}) - \phi_h^{n-1}(\mathbf{x}^n)| = |\phi_h^{n-1}(\mathbf{x}^n)| \text{ for some } \mathbf{y} \in \text{conv}(\mathbf{x}^{n-1}, \mathbf{x}^n).$$

For the same $\mathbf{y}$ we have $(\mathbf{x}^{n-1} - \mathbf{x}^n) \parallel \nabla \phi^{n-1}(\mathbf{y})$ which together with $|\nabla \phi^{n-1}| = 1$ and (20) yields

$$\begin{aligned}
(47) \qquad |\mathbf{x}^{n-1} - \mathbf{x}^n| &= |(\mathbf{x}^{n-1} - \mathbf{x}^n) \cdot \nabla \phi^{n-1}(\mathbf{y})| \\
&\leq |(\mathbf{x}^{n-1} - \mathbf{x}^n) \cdot \nabla \phi_h^{n-1}(\mathbf{y})| + |(\mathbf{x}^{n-1} - \mathbf{x}^n) \cdot \nabla \left(\phi^{n-1}(\mathbf{y}) - \phi_h^{n-1}(\mathbf{y}) \right)| \\
&\leq |\phi_h^{n-1}(\mathbf{x}^n)| + ch^q |\mathbf{x}^{n-1} - \mathbf{x}^n| = |\phi_h^{n-1}(\mathbf{x}^n) - \phi_h^n(\mathbf{x}^n)| + ch^q |\mathbf{x}^{n-1} - \mathbf{x}^n| \\
&\leq c\delta_n + ch^q |\mathbf{x}^{n-1} - \mathbf{x}^n| \quad \Longrightarrow \quad |\mathbf{x}^{n-1} - \mathbf{x}^n| \lesssim \frac{\delta_n}{1 - ch^q},
\end{aligned}$$

where for the last estimate we made use of (21a) and (24). We note that (47) estimates the 'distance' between Γ_h^n and Γ_h^{n-1} measured in the normal directions to Γ^{n-1}. From (10) we find

$$|(\mathbf{x}^n - \mathbf{x}^{n-1}) \cdot \nabla \kappa_i(\mathbf{y})| = |\mathbf{x}^n - \mathbf{x}^{n-1}| |\mathbf{n} \cdot \nabla \kappa_i(\mathbf{y})| = \kappa_i^2(\mathbf{y}) |\mathbf{x}^n - \mathbf{x}^{n-1}|$$

for any $\mathbf{y} \in \text{conv}(\mathbf{x}^{n-1}, \mathbf{x}^n)$. We use this to estimate,

$$\begin{aligned}
(48) \qquad |a_i^n - a_i^{n-1}| &= |\phi^{n-1}(\mathbf{x}^n) \kappa_i(\mathbf{x}^n) - \phi^{n-1}(\mathbf{x}^{n-1}) \kappa_i(\mathbf{x}^{n-1})| \\
&= |\nabla(\phi^{n-1}(\mathbf{y}) \kappa_i(\mathbf{y})) \cdot (\mathbf{x}^n - \mathbf{x}^{n-1})| \qquad \text{for some } \mathbf{y} \in \text{conv}(\mathbf{x}^{n-1}, \mathbf{x}^n), \\
&\leq |\nabla \phi^{n-1}(\mathbf{y})| |\kappa_i(\mathbf{y})| |\mathbf{x}^n - \mathbf{x}^{n-1}| + |\phi^{n-1}(\mathbf{y})| |(\mathbf{x}^n - \mathbf{x}^{n-1}) \cdot \nabla \kappa_i(\mathbf{y})| \\
&\leq |\kappa_i(\mathbf{y})| |\mathbf{x}^n - \mathbf{x}^{n-1}| + \underbrace{|\phi^{n-1}(\mathbf{y})| |\kappa_i(\mathbf{y})|}_{\lesssim \delta_n \kappa(\mathbf{y}) \lesssim 1} |\kappa_i(\mathbf{y})| |\mathbf{x}^n - \mathbf{x}^{n-1}| \lesssim c_\delta \|\kappa\|_{\infty, I_n} \|w_N\|_{\infty, I_n} \Delta t.
\end{aligned}$$

From (20), (47) and the smoothness of ϕ, $\|\phi\|_{C^2(\mathcal{G})} \leq c_\phi$ we also conclude

$$\begin{aligned}
(49) \qquad |b^{k-1} - b^k| &= |\mathbf{n}_h^{n-1}(\mathbf{x}^{n-1}) \cdot \mathbf{n}^{n-1}(\mathbf{x}^{n-1}) - \mathbf{n}_h^n(\mathbf{x}^n) \cdot \mathbf{n}^{n-1}(\mathbf{x}^n)| \\
&\leq |\mathbf{n}_h^{n-1}(\mathbf{x}^{n-1}) \cdot \mathbf{n}^{n-1}(\mathbf{x}^{n-1}) - \mathbf{n}_h^n(\mathbf{x}^n) \cdot \mathbf{n}^n(\mathbf{x}^n)| + |\mathbf{n}_h^n(\mathbf{x}^n) \cdot \overbrace{(\nabla \phi^n(\mathbf{x}^n) - \nabla \phi^{n-1}(\mathbf{x}^n))}^{=(\mathbf{n}^n(\mathbf{x}^n) - \mathbf{n}^{n-1}(\mathbf{x}^n))}| \\
&\lesssim |\mathbf{n}_h^{n-1}(\mathbf{x}^{n-1}) \cdot \mathbf{n}^{n-1}(\mathbf{x}^{n-1}) - \mathbf{n}_h^n(\mathbf{x}^n) \cdot \mathbf{n}^n(\mathbf{x}^n)| + c_\phi \Delta t \\
&\lesssim |\mathbf{n}_h^{n-1}(\mathbf{x}^{n-1}) - \mathbf{n}^{n-1}(\mathbf{x}^{n-1})|^2 + |\mathbf{n}_h^n(\mathbf{x}^n) - \mathbf{n}^n(\mathbf{x}^n)|^2 + c_\phi \Delta t \lesssim h^{2q} + c_\phi \Delta t,
\end{aligned}$$

where in the last step we made use of $|\mathbf{n}^k(\mathbf{x}^k)| = |\mathbf{n}_h^k(\mathbf{x}^k)| = 1$, $k = 1, 2$ and hence

$$\mathbf{n}_h^k(\mathbf{x}^k) \cdot \mathbf{n}^k(\mathbf{x}^k) = 1 - \frac{1}{2} |\mathbf{n}_h^k(\mathbf{x}^k) - \mathbf{n}^k(\mathbf{x}^k)|^2.$$

Plugging (48) and (49) into (46) and exploiting (43) completes the proof. $\qquad \square$

The following lemma is an analogue to Lemma 6, where a discrete normal gradient in the volume is used to replace the closest point projection.

LEMMA 7. *Under the conditions of Lemma 6 the following estimate holds for all $v_h \in V_h^{n-1}$,*

$$(50) \qquad \|v_h\|_{\Gamma_h^n}^2 \leq (1 + c_{7a} \Delta t) \|v_h\|_{\Gamma_h^{n-1}}^2 + c_{7b} \delta_n (\delta_n + h) \|\mathbf{n}_h \cdot \nabla v_h\|_{\mathcal{O}(\Gamma_h^{n-1})}^2,$$

for some c_{7a} and c_{7b} independent of h, Δt and n.

Proof. We first note that $\Gamma_h^n \subset \mathcal{O}(\Gamma_h^{n-1})$, cf. condition (28). From condition (28) and $\mathcal{O}(\Gamma_h^{n-1}) \subset \mathcal{O}(\Gamma^{n-1})$ we know that both Γ_h^n and Γ_h^{n-1} are in $\mathcal{O}(\Gamma^{n-1})$. Hence, we can define a lift $v^\ell \in L^2(\Gamma_h^n)$ for $v \in L^2(\Gamma_h^{n-1})$ along normal directions to Γ^{n-1}, i.e., $v^\ell(\mathbf{x}) = v^\ell(\mathbf{l}^{n-1,n}\mathbf{p}^{n-1}(\mathbf{x}))$, $\mathbf{x} \in \Gamma_h^n$. We start with the splitting

$$\|v_h\|_{\Gamma_h^n}^2 = \int_{\Gamma_h^n} (|v_h|^2 - |v_h^\ell|^2)\, d\mathbf{x} + \|v_h^\ell\|_{\Gamma_h^n}^2$$

and bound the first term on the right-hand side:

$$\int_{\Gamma_h^n} (|v_h|^2 - |v_h^\ell|^2)\, d\mathbf{s}$$

$$\lesssim \delta_n \int_{\mathcal{O}(\Gamma_h^{n-1})} \mathbf{n} \cdot \nabla(|v_h|^2 - |v_h^\ell|^2)\, d\mathbf{x} \qquad \text{(with (47), } v_h^2 = |v_h^\ell|^2 \text{ on } \Gamma_h^{n-1})$$

$$= \delta_n \int_{\mathcal{O}(\Gamma_h^{n-1})} \mathbf{n}_h \cdot \nabla|v_h|^2\, d\mathbf{x} + \delta_n \int_{\mathcal{O}(\Gamma_h^{n-1})} (\mathbf{n} - \mathbf{n}_h) \cdot \nabla|v_h|^2\, d\mathbf{x} \qquad (\text{as } \mathbf{n} \cdot \nabla|v_h^\ell|^2 = 0)$$

$$\lesssim \delta_n \|\mathbf{n}_h \cdot \nabla v_h\|_{\mathcal{O}(\Gamma_h^{n-1})} \|v_h\|_{\mathcal{O}(\Gamma_h^{n-1})} + \delta_n \|\mathbf{n} - \mathbf{n}_h\|_{\infty, \mathcal{O}(\Gamma_h^{n-1})} \|\nabla v_h\|_{\mathcal{O}(\Gamma_h^{n-1})} \|v_h\|_{\mathcal{O}(\Gamma_h^{n-1})}$$

$$\lesssim \delta_n(\delta_n + h)\|\mathbf{n}_h \cdot \nabla v_h\|_{\mathcal{O}(\Gamma_h^{n-1})}^2 + \delta_n(h^{q-1} + (\delta_n + h)^{-1})\|v_h\|_{\mathcal{O}(\Gamma_h^{n-1})}^2 \qquad (\text{Young, (20), FE inv. ineq.})$$

$$\lesssim \delta_n\big((\delta_n + h) + h^{q-1}(\delta_n + h)^2\big)\|\mathbf{n}_h \cdot \nabla v_h\|_{\mathcal{O}(\Gamma_h^{n-1})} + \delta_n\big(1 + h^{q-1}(\delta_n + h)\big)\|v_h\|_{\Gamma_h^{n-1}}^2 \qquad (\text{Thm. 5})$$

$$\lesssim \delta_n\Big((\delta_n + h)\|\mathbf{n}_h \cdot \nabla v_h\|_{\mathcal{O}(\Gamma_h^{n-1})}^2 + \|v_h\|_{\Gamma_h^{n-1}}^2\Big) \qquad (h^{q-1} \lesssim 1,\ \delta_n + h \lesssim 1)$$

Next, we apply (44), $\|v_h^\ell\|_{\Gamma_h^n}^2 \leq (1 + c_6\Delta t)\,\|v_h\|_{\Gamma_h^{n-1}}^2$ so that we obtain

$$\|v_h\|_{\Gamma_h^n}^2 \leq (1 + \underbrace{c_6\Delta t + c\delta_n}_{c_{7a}\Delta t})\|v_h\|_{\Gamma_h^{n-1}}^2 + c_{7b}\delta_n(\delta_n + h)\|\mathbf{n}_h \cdot \nabla v_h\|_{\mathcal{O}(\Gamma_h^{n-1})}^2. \qquad \square$$

5.3. Stability analysis. For the well-posedness and numerical stability we need some additional conditions on the discretization parameters. First, we formulate a condition on the time step size analogously to (7):

$$(51) \qquad \Delta t \leq (4\xi_h)^{-1} \text{ with } \xi_h := \max_{n=0,..,N} \|\operatorname{div}_{\Gamma_h}(\mathbf{w}^e - \tfrac{1}{2}\mathbf{w}_T^e)\|_{L^\infty(\Gamma_h(t_n))}.$$

From the definition of ξ_h and geometrical approximation condition (20), it follows that

$$(52) \qquad \xi_h \leq C_0,$$

with some C_0 independent of Δt and h.

For the stability analysis we formulate the following condition on ρ_n:

$$(53) \qquad \rho_n \geq c_\delta c_{7b} \|w_N\|_{\infty, I_n}(\delta_n + h),$$

with c_{7b} as in Lemma 7 (which is a constant independent of Δt and h). This condition and (24) imply $\rho_n\Delta t \geq c_{7b}\delta_n(\delta_n + h)$.

With conditions (43) and (53) fulfilled estimate (50) simplifies to

$$(54) \qquad \|v_h\|_{\Gamma_h^n}^2 \leq (1 + c_{7a}\Delta t)\|v_h\|_{\Gamma_h^{n-1}}^2 + \rho_n\Delta t\|\mathbf{n}_h \cdot \nabla v_h\|_{\mathcal{O}(\Gamma_h^{n-1})}^2, \quad v_h \in V_h^{n-1}.$$

For the notation convenience, we introduce the bilinear form,

$$a_n(u,v) := \int_{\Gamma_h^n} \left(\frac{1}{2}(\mathbf{w}_T^e \cdot \nabla_{\Gamma_h} u)v - \frac{1}{2}(\mathbf{w}_T^e \cdot \nabla_{\Gamma_h} v)u + (\operatorname{div}_{\Gamma_h}(\mathbf{w}^e - \frac{1}{2}\mathbf{w}_T^e))uv\right) ds$$

$$+ \nu \int_{\Gamma_h^n} (\nabla_{\Gamma_h} u) \cdot (\nabla_{\Gamma_h} v)\, ds + \rho_n \int_{\mathcal{O}(\Gamma_h^n)} (\mathbf{n}_h \cdot \nabla u)(\mathbf{n}_h \cdot \nabla v)\, d\mathbf{x}$$

for $u, v \in H^1(\mathcal{O}(\Gamma_h^n))$. We estimate $a_n(v_h, v_h)$ from below,

$$
\text{(55)} \quad
\begin{aligned}
a_n(v_h, v_h) &= \nu\|\nabla_{\Gamma_h} v_h\|_{\Gamma_h^n}^2 + ((\mathrm{div}_{\Gamma_h}(\mathbf{w}^e - \tfrac{1}{2}\mathbf{w}_T^e)v_h, v_h)_{\Gamma_h^n} + \rho_n\|\mathbf{n}_h \cdot \nabla v_h\|_{\mathcal{O}(\Gamma_h^n)}^2 \\
&\geq \nu\|\nabla_{\Gamma_h} v_h\|_{\Gamma_h^n}^2 - \xi_h\|v_h\|_{\Gamma_h^n}^2 + \rho_n\|\mathbf{n}_h \cdot \nabla v_h\|_{\mathcal{O}(\Gamma_h^n)}^2
\end{aligned}
$$

for any $v_h \in V_h^n$. Using (55) and (51) we check that the bilinear form on the left-hand side of (30) is positive definite,

$$
\text{(56)} \quad \int_{\Gamma_h^n} \frac{1}{\Delta t} v_h^2 \, ds + a_n(v_h, v_h) \geq \frac{1}{2\Delta t}\|v_h\|_{\Gamma_h^n}^2 + \nu\|\nabla_{\Gamma_h} v_h\|_{\Gamma_h^n}^2 + \rho_n\|\mathbf{n}_h \cdot \nabla v_h\|_{\mathcal{O}(\Gamma_h^n)}^2
$$

Hence, due to the Lax-Milgram lemma, the problem in each time step of (30) is well-posed.

We next derive an *a priori* estimate for the finite element solution to (30).

THEOREM 8. *Assume conditions* (26), (28), (43), (51) *and* (53), *then the solution of* (30) *satisfies the following estimate for Δt sufficiently small:*

$$
\text{(57)} \quad \|u_h^n\|_{\Gamma_h^n}^2 + \sum_{k=1}^n \Delta t\Big(2\nu\|\nabla_{\Gamma_h} u_h^k\|_{\Gamma_h^0}^2 + \rho_n\|\mathbf{n}_h \cdot \nabla u_h^k\|_{\mathcal{O}(\Gamma_h^k)}^2\Big) \leq \frac{3}{2}\exp(c_8 t_n)\Big(\|u_h^0\|_{\Gamma_h^0}^2 + \rho_1\|\mathbf{n}_h \cdot \nabla u_h^0\|_{\mathcal{O}(\Gamma_h^0)}^2\Big).
$$

with c_8 independent of h, Δt and n.

Proof. We test (30) with $v_h = u_h^n$. This leads us to the identity

$$
\frac{1}{2\Delta t}(\|u_h^n\|_{\Gamma_h^n}^2 + \|u_h^n - u_h^{n-1}\|_{\Gamma_h^n}^2) + a_n(u_h^n, u_h^n) = \frac{1}{2\Delta t}\|u_h^{n-1}\|_{\Gamma_h^n}^2.
$$

We drop out the second term, use the lower bound (55) and apply (54) and assumption (52)

$$
\text{(58)} \quad
\begin{aligned}
&\|u_h^n\|_{\Gamma_h^n}^2 + 2\Delta t\nu\|\nabla_{\Gamma_h} u_h^n\|_{\Gamma_h^n}^2 + 2\Delta t\rho_n\|\mathbf{n}_h \cdot \nabla u_h^n\|_{\mathcal{O}(\Gamma_h^n)}^2 \\
&\leq \|u_h^{n-1}\|_{\Gamma_h^n}^2 + 2\xi_h\Delta t\|u_h^n\|_{\Gamma_h^n}^2 \\
&\leq (1 + c_{7a}\Delta t\|u_h^{n-1}\|_{\Gamma_h^{n-1}}^2) + \Delta t\rho_n\|\mathbf{n}_h \cdot \nabla u_h^{n-1}\|_{\mathcal{O}(\Gamma_h^{n-1})}^2 + 2C_0\Delta t\|u_h^n\|_{\Gamma_h^n}^2
\end{aligned}
$$

where the constants c_{7a} and C_0 are independent of h, Δt and n. We define $c^* = c_{7a} + 2C_0$ and sum up the inequalities for $n = 1, \dots, k$ to get

$$
(1 - \Delta t c^*)\|u_h^k\|_{\Gamma_h^k}^2 + \Delta t\sum_{n=1}^k \Big(2\nu\|\nabla_{\Gamma_h} u_h^n\|_{\Gamma_h^n}^2 + \rho_n\|\mathbf{n}_h \cdot \nabla u_h^n\|_{\mathcal{O}(\Gamma_h^n)}^2\Big)
$$

$$
\leq \|u_h^0\|_{\Gamma^{n-1}}^2 + \rho_1\|\mathbf{n}_h \cdot \nabla u_h^0\|_{\mathcal{O}(\Gamma_h^0)}^2 + \Delta t\sum_{n=0}^{k-1} c^*\|u_h^n\|_{\Gamma_h^n}^2.
$$

Finally, we apply the discrete Gronwall inequality with $\Delta t \leq (2c^*)^{-1}$ to get (57) with $c_8 = 2c^*$. ☐

Now we are ready to devise an error estimate in the energy norm. The proof of the error estimate combines the arguments we used for stability analysis in section 5.3 with geometric and interpolation error estimates. The geometric and interpolation error estimates are treated at each time instances t_n for 'stationary' surfaces Γ_h^n and so the developed analysis (cf. [40, 34]) is of help. We start with consistency estimate for (30).

5.4. Consistency estimate. While stability analysis dictated us the lower bound (53) for ρ_n, we shall see that the consistency and error analysis leads to the following natural upper bound:

$$
\text{(59)} \quad \rho_n \lesssim (h + \delta_n)^{-1}.
$$

We assume (59) for the rest of section 5. Furthermore, in the consistency and error bounds we shall need estimates on derivatives of the solution u in the strip $\mathcal{O}(\mathcal{G})$. By differentiating the identity

$u(\mathbf{x}, t) = u(\mathbf{p}(\mathbf{x}), t)$, $(\mathbf{x}, t) \in \mathcal{O}(\mathcal{G})$, $k \geq 0$ times one finds that for C^{k+1}-smooth manifold $\mathcal{G}$ the following bound holds:

$$(60) \qquad \|u\|_{W^{k,\infty}(\mathcal{O}(\mathcal{G}))} \lesssim \|u\|_{W^{k,\infty}(\mathcal{G})}.$$

With a little bit more calculations, see, for example, [40, Lemma 3.1], one also finds

$$(61) \qquad \|u\|_{H^k(U_\varepsilon(\Gamma(t)))} \lesssim \varepsilon^{\frac{1}{2}} \|u\|_{H^k(\Gamma(t))}$$

for $t \in [0, T]$ and any such $\varepsilon > 0$ that $U_\varepsilon(\Gamma(t)) \subset \mathcal{O}(\Gamma(t))$, where $U_\varepsilon(\Gamma(t))$ is the ε-neighborhood in $\mathbb{R}^3$.

We next observe that the smooth solution $u^n = u(t_n)$ of (2) satisfy the identities

$$(62) \qquad \int_{\Gamma_h^n} \left(\frac{u^n - u^{n-1}}{\Delta t} \right) v_h \, ds + a_n(u^n, v_h) = \mathcal{E}_C^n(v_h), \quad \forall \, v_h \in V_h^n,$$

where $\mathcal{E}_C^n(v_h)$ collects consistency terms due to geometric errors and time derivative approximation, i.e.

$$\mathcal{E}_C^n(v_h) = \underbrace{\int_{\Gamma_h^n} \left(\frac{u^n - u^{n-1}}{\Delta t} \right) v_h \, ds_h - \int_{\Gamma^n} u_t(t_n) v_h^\ell \, ds}_{I_1} + \underbrace{\rho_n \int_{\mathcal{O}(\Gamma_h^n)} ((\mathbf{n}_h - \mathbf{n}) \cdot \nabla u^n)(\mathbf{n}_h \cdot \nabla v_h) d\mathbf{x}}_{I_2}$$

$$+ \underbrace{\frac{1}{2} \int_{\Gamma_h^n} \mathbf{w}_T^e \cdot \nabla_{\Gamma_h} u^n v_h - \mathbf{w}_T^e \cdot \nabla_{\Gamma_h} v_h u^n \, ds_h - \frac{1}{2} \int_{\Gamma^n} \mathbf{w} \cdot \nabla u^n v_h^\ell - \mathbf{w} \cdot \nabla v_h^\ell u^n \, ds}_{I_{3,a}}$$

$$+ \underbrace{\int_{\Gamma_h^n} \mathrm{div}_{\Gamma_h}(\mathbf{w}^e - \frac{1}{2}\mathbf{w}_T^e) u^n v_h \, ds_h - \int_{\Gamma^n} \mathrm{div}_\Gamma(\mathbf{w} - \frac{1}{2}\mathbf{w}_T) u^n v_h^\ell \, ds}_{I_{3,b}}$$

$$+ \underbrace{\nu \int_{\Gamma_h^n} \nabla_{\Gamma_h} u^n \cdot \nabla_{\Gamma_h} v_h \, ds_h - \nu \int_{\Gamma^n} \nabla_\Gamma u^n \cdot \nabla_\Gamma v_h^\ell \, ds}_{I_4}.$$

We give the estimate for consistency terms in the following lemma.

LEMMA 9. *Assume $u \in W^{2,\infty}(\mathcal{G})$, then consistency error has the bound*

$$(63) \qquad |\mathcal{E}_C^n(v_h)| \lesssim (\Delta t + h^q) \|u\|_{W^{2,\infty}(\mathcal{G})} \left(\|v_h\|_{\Gamma_h^n} + \nu^{\frac{1}{2}} \|\nabla_\Gamma v_h\|_{\Gamma_h^n} + \rho_n^{\frac{1}{2}} \|(\mathbf{n}_h \cdot \nabla v_h)\|_{\mathcal{O}(\Gamma_h^n)} \right).$$

Proof. We treat $\mathcal{E}_C^n(v_h)$ term by term, starting with I_1:

$$I_1 = -\int_{\Gamma_h^n} \int_{t_{n-1}}^{t_n} \frac{t - t_{n-1}}{\Delta t} u_{tt} \, dt \, v_h \, ds + \int_{\Gamma_h^n} u_t(t_n) v_h \, ds - \int_{\Gamma^n} u_t(t_n) v_h^\ell \, ds.$$

We have

$$\left| -\int_{\Gamma_h^n} \int_{t_{n-1}}^{t_n} u_{tt} \frac{t - t_{n-1}}{\Delta t} \, dt \, v_h \, ds \right| \leq \frac{1}{2} \Delta t \|u_{tt}\|_{\infty, \mathcal{O}(G)} \|v_h\|_{L^1(\Gamma_h^n)} \lesssim \Delta t \|u\|_{W^{2,\infty}(\mathcal{G})} \|v_h\|_{\Gamma_h^n},$$

and using $u_t^e(\mathbf{x}, t) = u_t(\mathbf{p}(\mathbf{x}), t) - \phi(\mathbf{x}, t) \mathbf{n}_t \cdot \nabla_\Gamma u(\mathbf{p}(\mathbf{x}), t)$ (cf. (6.8) in [33]),

$$\int_{\Gamma_h^n} u_t(t_n) v_h \, ds_h - \int_{\Gamma^n} u_t(t_n) v_h^\ell \, ds = \int_{\Gamma_h^n} \left((u_t \circ \mathbf{p})(1 - \mu_h) - \phi \mathbf{n}_t \cdot \nabla_\Gamma u \circ \mathbf{p} \right) v_h \, ds_h$$

$$\lesssim h^{q+1}(\|u_t\|_{\Gamma^n} + \|\nabla_\Gamma u\|_{\Gamma^n}) \|v_h\|_{\Gamma_h^n},$$

15

where we used (22), $\|\phi\|_{\infty,\Gamma_h^n} \lesssim h^{q+1}$, and $\mu_h^n(\mathbf{x})ds_h(\mathbf{x}) = ds(\mathbf{p}(\mathbf{x}))$, $\mathbf{x} \in \Gamma_h^n$, with $\|1 - \mu_h\|_{\infty,\Gamma_h^n} \lesssim h^{q+1}$; see, e.g., [40]. We now turn to estimating the second term,

$$
\begin{aligned}
|I_2| &\leq \rho_n \|(\mathbf{n}_h - \mathbf{n}) \cdot \nabla u^n\|_{\mathcal{O}(\Gamma_h^n)} \|\mathbf{n}_h \cdot \nabla v_h\|_{\mathcal{O}(\Gamma_h^n)} \\
&\lesssim \rho_n h^q \|\nabla u^n\|_{\mathcal{O}(\Gamma_h^n)} \|\mathbf{n}_h \cdot \nabla v_h\|_{\mathcal{O}(\Gamma_h^n)} \lesssim \rho_n h^q (\delta_n + h)^{\frac{1}{2}} \|\nabla_\Gamma u^n\|_{\Gamma_h^n} \|\mathbf{n}_h \cdot \nabla v_h\|_{\mathcal{O}(\Gamma_h^n)}.
\end{aligned}
$$

In the last inequality we used (61). Recalling the condition (59) for ρ_n, we find

$$
|I_2| \lesssim h^q \rho_n^{\frac{1}{2}} \|\nabla_\Gamma u^n\|_{\Gamma_h^n} \|\mathbf{n}_h \cdot \nabla v_h\|_{\mathcal{O}(\Gamma_h^n)}.
$$

The consistency terms $I_{3,a}$, $I_{3,b}$, I_4 are standard in TraceFEM on steady surfaces. One has the bounds, see [17, Lemma 7.4] or [40, Lemma 5.5],

$$
|I_{3,a}| + |I_4| \lesssim h^{q+1} \left(\|\nabla_\Gamma u^n\|_{\Gamma^n} \|v_h\|_{\Gamma_h^n} + \|\nabla_\Gamma u^n\|_{\Gamma^n} \|\nabla_{\Gamma_h} v_h\|_{\Gamma_h^n} \right).
$$

We fix $t = t_n$ and skip the dependence on time in our notation up to the end of the proof. To handle the term with divergence, introduce orthogonal projectors,

$$
\begin{aligned}
\mathbf{P}(\mathbf{x}) &:= \mathbf{I} - \mathbf{n}(\mathbf{x})\mathbf{n}(\mathbf{x})^T, \quad \text{for } \mathbf{x} \in \mathcal{O}(\Gamma^n), \\
\mathbf{P}_h(\mathbf{x}) &:= \mathbf{I} - \mathbf{n}_h(\mathbf{x})\mathbf{n}_h(\mathbf{x})^T, \quad \text{for } \mathbf{x} \in \Gamma_h^n.
\end{aligned}
$$

For the surface divergence one has the following representation:

$$
(64) \qquad \operatorname{div}_\Gamma \mathbf{w} = \operatorname{tr}(\nabla_\Gamma \mathbf{w}) = \operatorname{tr}(\mathbf{P}\nabla \mathbf{w}) \quad \text{and} \quad \operatorname{div}_{\Gamma_h} \mathbf{w} = \operatorname{tr}(\nabla_{\Gamma_h} \mathbf{w}) = \operatorname{tr}(\mathbf{P}_h \nabla \mathbf{w}).
$$

Take $\mathbf{x} \in \Gamma_h$, not lying on an edge. Using $\nabla u(\mathbf{x}) = (\mathbf{I} - \phi(\mathbf{x})\mathbf{H})\nabla_\Gamma u(\mathbf{p}(\mathbf{x}))$, $\mathbf{x} \in \mathcal{O}(\Gamma^n)$, we obtain

$$
\begin{aligned}
\operatorname{div}_{\Gamma_h} \mathbf{w}^e(\mathbf{x}) &= \operatorname{tr}(\mathbf{P}_h \nabla \mathbf{w}^e(\mathbf{x})) = \operatorname{tr}\left(\mathbf{P}_h(\mathbf{I} - \phi(\mathbf{x})\mathbf{H})\nabla_\Gamma \mathbf{w}(\mathbf{p}(\mathbf{x}))\right) \\
&= \operatorname{tr}\left(\mathbf{P}\nabla_\Gamma \mathbf{w}(\mathbf{p}(\mathbf{x}))\right) + \operatorname{tr}\left((\mathbf{P}_h - \mathbf{P})\nabla_\Gamma \mathbf{w}(\mathbf{p}(\mathbf{x}))\right) - \phi(\mathbf{x})\operatorname{tr}\left(\mathbf{P}_h \mathbf{H}\nabla_\Gamma \mathbf{w}(\mathbf{p}(\mathbf{x}))\right) \\
&= \operatorname{div}_\Gamma \mathbf{w}(\mathbf{p}(\mathbf{x})) + \operatorname{tr}\left((\mathbf{P}_h - \mathbf{P})\nabla_\Gamma \mathbf{w}(\mathbf{p}(\mathbf{x}))\right) - \phi(\mathbf{x})\operatorname{tr}\left(\mathbf{P}_h \mathbf{H}\nabla_\Gamma \mathbf{w}(\mathbf{p}(\mathbf{x}))\right).
\end{aligned}
$$

Thanks to (22) and (23), we bound the last two terms at the right-hand side

$$
|\mathbf{P}_h - \mathbf{P}| \lesssim h^q, \quad |\phi(\mathbf{x})\mathbf{P}_h \mathbf{H}| \lesssim h^{q+1}.
$$

We proved the estimate $|\operatorname{div}_{\Gamma_h} \mathbf{w}^e - \operatorname{div}_\Gamma \mathbf{w} \circ \mathbf{p}| \lesssim h^q$ on Γ_h^n. With the help of this estimate and the similar one with $\mathbf{w}$ replaced by $\mathbf{w}_T$, we bound $I_{3,b}$ term,

$$
\begin{aligned}
|I_{3,b}| &= \left| \int_{\Gamma_h^n} \left(\operatorname{div}_{\Gamma_h}(\mathbf{w}^e - \tfrac{1}{2}\mathbf{w}_T^e) - \mu_h \operatorname{div}_\Gamma(\mathbf{w} - \tfrac{1}{2}\mathbf{w}_T) \circ \mathbf{p} \right) u^n v_h \, ds_h \right| \\
&\lesssim h^q \|u^n\|_{\Gamma^n} \|v_h\|_{\Gamma_h^n}.
\end{aligned}
$$

$\square$

REMARK 5.1. The h-dependence of the consistency estimate in (63) is due to the geometric errors. Increasing the accuracy of the surface recovery leads to better consistency in (63). The order of the estimate can be improved with respect to h if more information about Γ is available. For example, if one can use $(\operatorname{div}_\Gamma(\mathbf{w} - \tfrac{1}{2}\mathbf{w}_T))^e$ instead of $\operatorname{div}_{\Gamma_h}(\mathbf{w}^e - \tfrac{1}{2}\mathbf{w}_T^e)$ on Γ_h, then the $O(h^q)$ term on the right-hand side of (63) is replaced by $O(h^{q+1})$.

5.5. Error estimate in the energy norm. Denote the error function $\mathbb{E}^n = u^n - u_h^n$, $\mathbb{E}^n \in H^1(\mathcal{O}(\Gamma_h^n))$. From (30) and (62) we get the error equation,

$$
(65) \qquad \int_{\Gamma_h^n} \left(\frac{\mathbb{E}^n - \mathbb{E}^{n-1}}{\Delta t} \right) v_h \, ds + a_n(\mathbb{E}^n, v_h) = \mathcal{E}_C^n(v_h), \quad \forall \, v_h \in V_h^n,
$$

We let $u_I^n \in V_h^n$ be an interpolant for u^n in $\mathcal{O}(\Gamma_h^n)$; we assume u^n sufficiently smooth so that the interpolation is well-defined. Following standard lines of argument, we split $\mathbb{E}^n$ into finite element and approximation parts,

$$
\mathbb{E}^n = \underbrace{(u^n - u_I^n)}_{e^n} + \underbrace{(u_I^n - u_h^n)}_{e_h^n}.
$$

Equation (65) yields

$$(66) \qquad \int_{\Gamma_h^n} \left(\frac{e_h^n - e_h^{n-1}}{\Delta t} \right) v_h \, ds + a_n(e_h^n, v_h) = \mathcal{E}_I^n(v_h) + \mathcal{E}_C^n(v_h), \quad \forall \, v_h \in V_h^n,$$

with the interpolation term

$$\mathcal{E}_I^n(v_h) = -\int_{\Gamma_h^n} \left(\frac{e^n - e^{n-1}}{\Delta t} \right) v_h \, ds_h - a_n(e^n, v_h).$$

We give the estimate for interpolation terms in the following lemma.

LEMMA 10. *Assume $u \in W^{m+1,\infty}(\mathcal{G})$ and $\mathcal{G}$ is sufficiently smooth, then it holds*

$$(67) \qquad |\mathcal{E}_I^n(v_h)| \lesssim h^m \|u\|_{W^{m+1,\infty}} (\|v_h\|_{\Gamma_h^n} + \nu^{\frac{1}{2}} \|\nabla_{\Gamma_h} v_h\|_{\Gamma_h^n}).$$

Proof. We need Hansbo's trace inequality [20],

$$(68) \qquad \|v\|_{S \cap \Gamma_h^n} \le c(h^{-\frac{1}{2}} \|v\|_S + h^{\frac{1}{2}} \|\nabla v\|_S), \qquad v \in H^1(S), \; S \in \mathcal{T}_h^\Gamma,$$

with some c independent of v, T, h, Γ_h^n. Under mild assumptions on the resolution of the smooth surface Γ_h^n by the mesh (cf. [40, Assumption 4.1(A2)]) the inequality has been proven in [40, Lemma 4.3]. We use interpolation properties of polynomials and their traces. In particular,

$$(69) \qquad \min_{v_h \in V^h} \left(\|v^e - v_h\|_{\Gamma_h^n} + h \|\nabla(v^e - v_h)\|_{\Gamma_h^n} \right) \lesssim h^{m+1} \|v\|_{H^{m+1}(\Gamma^n)} \quad \text{for } v \in H^{m+1}(\Gamma^n);$$

see, e.g., [17, 40, 34]. With the help of (68) we treat the first term in $\mathcal{E}_I^n(v_h)$,

$$(70) \qquad \begin{aligned} \left| \int_{\Gamma_h^n} \left(\frac{e^n - e^{n-1}}{\Delta t} \right) v_h \, ds_h \right| &\le \left\| \frac{e^n - e^{n-1}}{\Delta t} \right\|_{\Gamma_h^n} \|v_h\|_{\Gamma_h^n} \\ &\lesssim \left(h^{-\frac{1}{2}} \Delta t^{-1} \|e^n - e^{n-1}\|_{\mathcal{O}_\Gamma(\Gamma_h^n)} + h^{\frac{1}{2}} \Delta t^{-1} \|\nabla(e^n - e^{n-1})\|_{\mathcal{O}_\Gamma(\Gamma_h^n)} \right) \|v_h\|_{\Gamma_h^n}. \end{aligned}$$

Now, using condition (28) we handle the first term on the right-hand side of (70),

$$\|e^n - e^{n-1}\|_{\mathcal{O}_\Gamma(\Gamma_h^n)}^2 = \|e(t_n) - e(t_{n-1})\|_{\mathcal{O}_\Gamma(\Gamma_h^n)}^2 = \left\| \int_{t_{n-1}}^{t_n} e_t(t') \, dt' \right\|_{\mathcal{O}_\Gamma(\Gamma_h^n)}^2$$

$$\le \Delta t \int_{t_{n-1}}^{t_n} \|e_t(t')\|_{\mathcal{O}_\Gamma(\Gamma_h^n)}^2 \, dt' \lesssim |\Delta t|^2 \, h^{2m} \sup_{t \in [t_{n-1}, t_n]} \|u_t\|_{H^m(\mathcal{O}_\Gamma(\Gamma_h^n))}^2 \qquad \text{(Cauchy-Schwarz and (69))}$$

$$\lesssim |\Delta t|^2 \, h^{2m+1} \sup_{t \in [t_{n-1}, t_n]} \|u_t\|_{H^m(\Gamma_h^n)}^2 \lesssim |\Delta t|^2 \, h^{2m+1} \|u\|_{W^{m+1,\infty}(\mathcal{G})}^2. \qquad \text{(by (61))}$$

We estimate the second term on the right-hand side of (70), using similar arguments,

$$\|\nabla(e^n - e^{n-1})\|_{\mathcal{O}_\Gamma(\Gamma_h^n)} \lesssim |\Delta t|^2 \, h^{2m-1} \|u\|_{W^{m+1,\infty}(\mathcal{G})}^2.$$

We handle the term $a_n(e^n, v_h)$ using the Cauchy-Schwarz inequality and interpolation properties of v_h in the straight-forward way. This leads to the estimate

$$|a_n(e^n, v_h)| \lesssim h^m \|u\|_{H^{m+1}(\Gamma^n)} (\|v_h\|_{\Gamma_h^n} + \nu^{\frac{1}{2}} \|\nabla_{\Gamma_h} v_h\|_{\Gamma_h^n}).$$

We summarize the above bounds into the estimate of the interpolation term as in (67). $\qquad \square$

Now we are prepared to prove the main result of the paper. Let $u_h^0 = u_I^0 \in V_h^0$ be a suitable interpolant to $u^0 \in \mathcal{O}(\Gamma_h^0)$.

THEOREM 11. *Assume* (20)–(21b), (26)–(28), (43), (51), (53), *and* (59), *and* Δt *is sufficiently small,* u *is the solution to* (1), $u \in W^{m+1,\infty}(\mathcal{G})$, $m \geq 1$, $\mathcal{G}$ *is sufficiently smooth. For* u_h^n, $n = 1, \ldots, N$, *the finite element solution of* (30), *and* $\mathbb{E}^n = u_h^n - u^n$ *the following error estimate holds:*

$$(71) \quad \|\mathbb{E}^n\|_{\Gamma_h^n}^2 + \Delta t \sum_{k=1}^n \left(\nu \|\nabla_{\Gamma_h} \mathbb{E}^k\|_{\Gamma_h^k}^2 + \rho_n \|\mathbf{n}_h \cdot \nabla \mathbb{E}_h^k\|_{\mathcal{O}(\Gamma_h^k)}^2 \right) \lesssim \exp(c_{11} t_n) R(u) (\Delta t^2 + h^{2 \min\{m,q\}}),$$

with $R(u) := \|u\|_{W^{m+1,\infty}(\mathcal{G})}^2$ *and* c_{11} *independent of* h, Δt, n *and of the position of the surface over the background mesh.*

Proof. The arguments largely repeat those used to show the stability result in Theorem 8 and involve estimates from Lemmas 9 and 10 to bound the arising right-hand side terms. We set $v_h = 2\Delta t e_h^n$ in (66). This gives

$$\|e_h^n\|_{\Gamma_h^n}^2 - \|e_h^{n-1}\|_{\Gamma_h^n}^2 + \|e_h^n - e_h^{n-1}\|_{\Gamma_h^n}^2 + 2\Delta t a_n(e_h^n, e_h^n) = 2\Delta t(\mathcal{E}_I^n(e_h) + \mathcal{E}_C^n(e_h))$$

Dropping the third term, using the lower bound (55) for a_n and estimating $\|e_h^{n-1}\|_{\Gamma_h^n}^2$ with (54) yields

$$\|e_h^n\|_{\Gamma_h^n}^2 + 2\Delta t\nu \|\nabla_{\Gamma_h} e_h^n\|_{\Gamma_h^n}^2 + 2\Delta t\rho_n \|\mathbf{n}_h \cdot \nabla e_h^n\|_{\mathcal{O}(\Gamma_h^n)}^2$$
$$\leq (1 + c_7^* \Delta t)\|e_h^{n-1}\|_{\Gamma^{n-1}}^2 + \Delta t\rho_n \|\mathbf{n}_h \cdot \nabla e_h^{n-1}\|_{\mathcal{O}(\Gamma_h^{n-1})}^2 + 2\xi_h \Delta t\|e_h^n\|_{\Gamma_h^n}^2 + 2\Delta t(\mathcal{E}_I^n(e_h) + \mathcal{E}_C^n(e_h)).$$

We recall assumption (52) and the definition $c^* = c_7^* + 2C_0$ (cf. the proof of Theorem 8) to obtain

$$(72) \quad (1 - c^*\Delta t)\|e_h^n\|_{\Gamma_h^n}^2 + 2\Delta t\nu \|\nabla_{\Gamma_h} e_h^n\|_{\Gamma_h^n}^2 + 2\Delta t\rho_n \|\mathbf{n}_h \cdot \nabla e_h^n\|_{\mathcal{O}(\Gamma_h^n)}^2$$
$$\leq (1 + c^*\Delta t)\|e_h^{n-1}\|_{\Gamma^{n-1}}^2 + \Delta t\rho_n \|\mathbf{n}_h \cdot \nabla e_h^{n-1}\|_{\mathcal{O}(\Gamma_h^{n-1})}^2 + 2\Delta t(\mathcal{E}_I^n(e_h) + \mathcal{E}_C^n(e_h)).$$

To estimate the interpolation and consistency terms, we apply Young's inequality to the right-hand sides of (63) and (67) yielding

$$2\Delta t\mathcal{E}_C^n(e_h) \leq c\,\Delta t(\Delta t^2 + h^{2q})\|u\|_{W^{2,\infty}(\mathcal{G})}^2 \quad + \frac{\Delta t}{2}\left(\|e_h^n\|_{\Gamma_h^n}^2 + \nu \|\nabla_{\Gamma_h} e_h^n\|_{\Gamma_h^n}^2 + \rho_n \|(\mathbf{n}_h \cdot \nabla e_h^n)\|_{\mathcal{O}(\Gamma_h^n)}^2 \right),$$

$$2\Delta t\mathcal{E}_I^n(e_h) \leq c\,\Delta t\,h^{2m}\|u\|_{W^{m+1,\infty}(\mathcal{G})}^2 \quad + \frac{\Delta t}{2}\left(\|e_h^n\|_{\Gamma_h^n}^2 + \nu \|\nabla_{\Gamma_h} e_h^n\|_{\Gamma_h^n}^2 \right),$$

with a constant c independent of h, Δt, n and of the position of the surface over the background mesh. Substituting this in (72) and summing up the resulting inequalities for $n = 1, \ldots, k$ and noting $e_h^0 = 0$ in $\mathcal{O}(\Gamma_h^0)$ we get

$$(1 - (c^* + 1)\Delta t)\|e_h^k\|_{\Gamma_h^k}^2 + \Delta t \sum_{n=1}^k \left(\nu \|\nabla_{\Gamma_h} e_h^n\|_{\Gamma_h^n}^2 + \rho_n \|\mathbf{n}_h \cdot \nabla e_h^n\|_{\mathcal{O}(\Gamma_h^n)}^2 \right)$$
$$\leq \Delta t \sum_{n=0}^{k-1} c^* \|e_h^n\|_{\Gamma_h^n}^2 + c\,\|u\|_{W^{m+1,\infty}}(\Delta t^2 + h^{2q} + h^{2m}).$$

We apply the discrete Gronwall inequality with $\Delta t \leq (2 + 2c^*)^{-1}$ to get

$$(73) \qquad \|e_h^k\|_{\Gamma_h^k}^2 + \sum_{n=1}^k \Delta t \left(\nu \|\nabla_{\Gamma_h} e_h^n\|_{\Gamma_h^n}^2 + \rho_n \|\mathbf{n}_h \cdot \nabla e_h^n\|_{\mathcal{O}(\Gamma_h^n)}^2 \right)$$
$$\lesssim \exp(c_{11} t_k)\|u\|_{W^{m+1,\infty}(\mathcal{G})}(\Delta t^2 + h^{2 \min\{m,q\}}) =: \exp(c_{11} t_k) Q_e,$$

with $c_{11} = 2(c^* + 1)$. Now the triangle inequality, standard FE interpolation properties, (69) and

18

(59) give

$$\|\mathbb{E}^k\|_{\Gamma_h^k}^2 + \sum_{n=1}^{k} \Delta t \left(\nu \|\nabla_{\Gamma_h} \mathbb{E}^n\|_{\Gamma_h^n}^2 + \rho_n \|\mathbf{n}_h \cdot \nabla \mathbb{E}^n\|_{\mathcal{O}(\Gamma_h^n)}^2 \right)$$

$$\leq Q_e + \|e^k\|_{\Gamma_h^k}^2 + \sum_{n=1}^{k} \Delta t \left(\nu \|\nabla_{\Gamma_h} e^n\|_{\Gamma_h^n}^2 + \rho_n \|\mathbf{n}_h \cdot \nabla e^n\|_{\mathcal{O}(\Gamma_h^n)}^2 \right)$$

$$\lesssim Q_e + \|u\|_{H^{m+1}(\Gamma^k)} h^{2m} \underbrace{(1 + \rho_n(\delta_n + h))}_{\lesssim 1}.$$

This completes the proof. □

REMARK 5.2 (Extension of the analysis to BDF2). The method is extendable to higher order time stepping methods. To keep the analysis manageable, we restricted to the backward Euler discretization. Here, we briefly summarize what needs to be considered for an extension of the analysis to higher order schemes. We consider the BDF2 schemes here. Obviously the finite difference stencil for the time derivative is changed from $\frac{u^n - u^{n-1}}{\Delta t}$ to $\frac{3u^n - 4u^{n-1} + u^{n-2}}{2\Delta t}$ in the semi-discrete method in (5),(6) and for the fully discrete method in (30). Accordingly, the layer width of the extension has be increased so that $\Gamma^n \subset \mathcal{O}(\Gamma^{n-1}) \cap \mathcal{O}(\Gamma^{n-2})$ and $\Gamma_h^n \subset \mathcal{O}(\Gamma_h^{n-1}) \cap \mathcal{O}(\Gamma_h^{n-1})$. To this end, we have to change δ_n in (24) to $\delta_n = 2c_\delta \sup_{t \in [t_{n-2}, t_n]} \|w_N\|_{L^\infty(\Gamma(t))} \Delta t$. Further, in the proof of the coercivity in the (spatially) continuous and discrete setting we have to change the time step restrictions (7) and (51) according to the changed coefficient in the BDF formula. The Gronwall-type arguments in section 3.3 and in Theorem 8 have to be replaced with corresponding versions for the BDF scheme. To handle the time derivative terms, a special norm should be used [19], which is a linear combination of L^2 surface norm at n and $n-1$ time steps. Finally, the consistency analysis in section 5.4 can then be improved, specifically the term I_1 leading to a higher order (in Δt) estimate in Lemma 9 and Theorem 11.

6. Algebraic stability. In every time step we have to solve a linear system of the form

$$\mathbf{A}\mathbf{x} = \mathbf{f} \quad \text{with } \mathbf{A} \in \mathbb{R}^{N \times N}, \mathbf{f}, \mathbf{x} \in \mathbb{R}^N,$$

where $N = \dim(V_h^n)$, $\mathbf{A}$ and $\mathbf{f}$ are the matrix and vector corresponding to the involved bilinear form and the right-hand side linear form, whereas $\mathbf{x}$ is the solution vector. We split the left-hand side bilinear form into its symmetric and skew-symmetric part and define

(74a) $\quad A_n(u,v) := B_n(u,v) + C_n(u,v) \quad \left(= \int_{\Gamma_h^n} \frac{1}{\Delta t} uv \, ds + a_n(u,v) \right), \qquad u, v \in V_h^n,$

(74b) $\quad B_n(u,v) := \int_{\Gamma_h^n} \left(\frac{1}{\Delta t} + \text{div}_{\Gamma_h}(\mathbf{w}^e - \frac{1}{2}\mathbf{w}_T^e) \right) uv \, ds$

$$+ \nu \int_{\Gamma_h^n} (\nabla_{\Gamma_h} u) \cdot (\nabla_{\Gamma_h} v) \, ds + \rho_n \int_{\mathcal{O}(\Gamma_h^n)} (\mathbf{n}_h \cdot \nabla u)(\mathbf{n}_h \cdot \nabla v) d\mathbf{x}, \qquad u, v \in V_h^n,$$

(74c) $\quad C_n(u,v) := \int_{\Gamma_h^n} \frac{1}{2}(\mathbf{w}_T^e \cdot \nabla_{\Gamma_h} u)v - \frac{1}{2}(\mathbf{w}_T^e \cdot \nabla_{\Gamma_h} v)u \, ds, \qquad u, v \in V_h^n.$

Correspondingly we denote by $\mathbf{B}$ and $\mathbf{C} \in \mathbb{R}^{N \times N}$ the matrices to the bilinear forms B_n and C_n.

To bound the spectral condition number of $\mathbf{A}$ we use the following result from the literature:

LEMMA 12. *With $\mathbf{A} \in \mathbb{R}^{N \times N}$, $\mathbf{B} = \frac{1}{2}(\mathbf{A} + \mathbf{A}^T)$ and $\mathbf{C} = \frac{1}{2}(\mathbf{A} - \mathbf{A}^T)$, for the spectral condition number of $\mathbf{A}$ there holds*

(75) $$\kappa(\mathbf{A}) \leq \frac{\lambda_{\max}(\mathbf{B}) + \rho_n(\mathbf{C})}{\lambda_{\min}(\mathbf{B})}$$

where $\rho_n(\cdot)$ denotes the spectral radius and $\lambda_{\max}(\mathbf{B})$ and $\lambda_{\min}(\mathbf{B})$ are the largest and smallest eigenvalues of the symmetric and positive definite matrix $\mathbf{B}$.

Proof. A proof is given in [12, Theorem 1]. □

To derive bounds for $\kappa(\mathbf{A})$ we derive bounds for $\rho(\mathbf{C})$ and $\lambda_{\min}(\mathbf{B})$ and $\lambda_{\max}(\mathbf{B})$ in the next two lemmas.

LEMMA 13. *There holds*

$$\rho_n(\mathbf{C}) \lesssim \|\mathbf{w}\|_\infty h^{d-2}. \tag{76}$$

Proof. We note that $\mathbf{C}$ is skew-symmetric and hence a normal matrix. Thus, we have

$$\rho_n(\mathbf{C}) = \max_{\mathbf{x} \in \mathbb{C}^N} \frac{\mathbf{x}^T \mathbf{C} \mathbf{x}}{\mathbf{x}^T \mathbf{x}}. \tag{77}$$

Now let $\mathbf{x} \in \mathbb{C}^n$ and v be the corresponding finite element function in $V_h + iV_h$ (where i is the imaginary unit), then we have

$$\mathbf{x}^T \mathbf{C} \mathbf{x} = C_n(v,v) \le \|\mathbf{w}\|_\infty \|\nabla_\Gamma v\|_{\Gamma_h} \|v\|_{\Gamma_h} \lesssim \|\mathbf{w}\|_\infty h^{-2} \|v\|_{\mathcal{O}(\Gamma_h^n)} \simeq \|\mathbf{w}\|_\infty h^{d-2} \|\mathbf{x}\|_2^2, \tag{78}$$

where we made use of inverse inequalities and $\|v\|_{\mathcal{O}(\Gamma_h^n)} \simeq h^d \|\mathbf{x}\|_2^2$. □

LEMMA 14. *Under conditions* (26) *and* (51), *there holds*

$$\lambda_{\max}(\mathbf{B}) \lesssim h^{d-2} \left(\frac{h}{\Delta t} + \frac{\nu}{h} + \rho_n \right), \tag{79a}$$

$$\lambda_{\min}(\mathbf{B}) \gtrsim h^d \left((\delta_n + h) \left(\Delta t + \frac{\delta_n + h}{\rho_n} \right) \right)^{-1}. \tag{79b}$$

Proof. Estimate (79a) follows with (51), $\Delta t < (4\xi_h)^{-1}$, standard FE inverse and trace inequalities similar to (78). Then again, with (56) and Theorem 5 we easily obtain (79b) with

$$h^d \|\mathbf{x}\|_2^2 \simeq \|u\|_{\mathcal{O}(\Gamma_h^n)}^2 \lesssim (\delta_n + h) \|u\|_{\Gamma_h^n}^2 + (\delta_n + h)^2 \|\mathbf{n}_h \cdot \nabla u\|_{\mathcal{O}(\Gamma_h^n)}^2 \tag{80}$$

$$\le (\delta_n + h) \max \left\{ \Delta t, \frac{\delta_n + h}{\rho_n} \right\} \cdot B_n(u,u) \le (\delta_n + h) \left(\Delta t + \frac{\delta_n + h}{\rho_n} \right) \cdot \underbrace{B_n(u,u)}_{=\mathbf{x}^T \mathbf{B} \mathbf{x}}. \quad □$$

COROLLARY 15. *The estimates in Lemma 13 and Lemma 14 plugged into Lemma 12 result in the following condition number bound:*

$$\kappa(\mathbf{A}) \lesssim \underbrace{\frac{\delta_n + h}{h}}_{K_1} \Bigg(\underbrace{\frac{1}{\Delta t} + \frac{\nu}{h^2} + \frac{\|\mathbf{w}\|_\infty}{h}}_{K_{2,a}} + \underbrace{\frac{\rho_n}{h}}_{K_{2,b}} \Bigg) \underbrace{\left(\Delta t + \frac{\delta_n + h}{\rho_n} \right)}_{K_3} \tag{81}$$

REMARK 6.1 (Discussion of Corollary 15). Let us discuss the terms on the r.h.s. of (81). The first term, K_1 describes the layer thickness in terms of elements. We note that this term is bounded by a constant for $\Delta t \lesssim h$. Otherwise the condition number will increase with an increasing (element) layer thickness. In the second term, $K_2 = K_{2,a} + K_{2,b}$, we first note that the latest contribution $K_{2,b} = \frac{\rho_n}{h}$ can be absorbed by $\frac{\nu}{h^2}$ if condition (59) is fulfilled and $\nu = \mathcal{O}(1)$. For the last term, K_3, we can use condition (53) to bound $K_3 \lesssim 1$. Assume Δt is the dominating summand in K_3. Then, there holds $K_2 \cdot K_3 \simeq 1 + \frac{\nu \Delta t}{h^2} + \frac{\|\mathbf{w}\|_\infty \Delta t}{h}$ which is the usual condition number scaling known from fitted convection diffusion equation discretizations on stationary domains which is the best that we can expect in our setting. We conclude that it is desirable to choose ρ_n sufficiently large so that $\rho_n \gtrsim \frac{\delta_n + h}{\Delta t}$. In view of (59) this however is only possible if $\Delta t \gtrsim h^2$. Next, we discuss possible choices for ρ_n and resulting scalings of the condition number.

6.1. Choices for ρ_n. We want to make a choice for ρ_n based on the stability, consistency and conditioning analysis. For the ease of presentation we set $\nu, \|\mathbf{w}\|_\infty = \mathcal{O}(1)$ in this paragraph and recall $\delta_n \simeq \|w_N\|_{\infty, I_n} \Delta t$. From the stability analysis and consistency analysis we have conditions (53) and (59), yielding the bounds

$$(\delta_n + h) \lesssim \rho_n \lesssim (\delta_n + h)^{-1}. \tag{82}$$

We consider three scalings: $\rho_n \sim 1$ and the limit cases $\rho_n \sim (\delta_n + h)^{-1}$ and $\rho_n \sim (\delta_n + h)$. In all these three cases we have $K_{2,b} \lesssim K_{2,a}$, i.e. $K_2 \simeq K_{2,a}$.

TABLE 1
$L^2(H^1)$- and $L^2(L^2)$-norm error in Experiment 1 with backward Euler and $\rho_n = 4$.

	$L^2(H^1)$-norm of the error				$L^2(L^2)$-norm of the error			
	$h = 1/2$	$h = 1/4$	$h = 1/8$	$h = 1/16$	$h = 1/2$	$h = 1/4$	$h = 1/8$	$h = 1/16$
$\Delta t = 1/8$	$\underline{9.3 \cdot 10^{-1}}$	$6.1 \cdot 10^{-1}$	$3.8 \cdot 10^{-1}$	$2.4 \cdot 10^{-1}$	$\underline{1.9 \cdot 10^{-1}}$	$9.9 \cdot 10^{-2}$	$1.2 \cdot 10^{-1}$	$1.4 \cdot 10^{-1}$
$\Delta t = 1/32$	$9.2 \cdot 10^{-1}$	$\underline{6.3 \cdot 10^{-1}}$	$3.5 \cdot 10^{-1}$	$1.8 \cdot 10^{-1}$	$2.7 \cdot 10^{-1}$	$\underline{1.2 \cdot 10^{-1}}$	$3.2 \cdot 10^{-2}$	$3.5 \cdot 10^{-2}$
$\Delta t = 1/128$	$9.2 \cdot 10^{-1}$	$6.4 \cdot 10^{-1}$	$\underline{3.5 \cdot 10^{-1}}$	$1.8 \cdot 10^{-1}$	$3.0 \cdot 10^{-1}$	$1.4 \cdot 10^{-1}$	$\underline{2.7 \cdot 10^{-2}}$	$1.0 \cdot 10^{-2}$
$\Delta t = 1/512$	$9.2 \cdot 10^{-1}$	$6.4 \cdot 10^{-1}$	$3.5 \cdot 10^{-1}$	$\underline{1.8 \cdot 10^{-1}}$	$3.1 \cdot 10^{-1}$	$1.4 \cdot 10^{-1}$	$3.0 \cdot 10^{-2}$	$\underline{7.4 \cdot 10^{-3}}$

1. Scaling $\rho_n \sim \delta_n + h$. There holds $K_3 \simeq 1$ so that the best bound is $\kappa(\mathbf{A}) \lesssim K_1 K_{2,a}$. For the special cases $\Delta t \sim h$ and $\Delta t \sim h^2$, this gives $\kappa(\mathbf{A}) \lesssim h^{-2}$

2. Scaling $\rho_n \sim 1$. Now, we have $K_3 \simeq \Delta t + h$ so that the best bound is $\kappa(\mathbf{A}) \lesssim K_1 K_{2,a}(\Delta t + h)$. This is already an improvement over the previous scaling as it predicts $\kappa(\mathbf{A}) \lesssim h^{-1}$ for the special cases $\Delta t \sim h$ and $\Delta t \sim h^2$.

3. Scaling $\rho_n \sim (\delta_h + h)^{-1}$. Finally, we have $K_3 \simeq \Delta t + h^2$ so that the best bound is $\kappa(\mathbf{A}) \lesssim K_1 K_{2,a}(\Delta t + h^2)$. For the cases $\Delta t \sim h$ this gives the same prediction as in the previous scaling, $\kappa(\mathbf{A}) \lesssim h^{-1}$. However, for $\Delta t \sim h^2$ we have the optimal bound $\kappa(\mathbf{A}) \lesssim 1$.

In the numerical experiments below we consider two choices

$$\text{(83a)} \qquad \qquad \rho_n \sim 1,$$

$$\text{(83b)} \qquad \qquad \rho_n \sim \frac{\nu}{\delta_h + h} + \|\mathbf{w}\|_\infty,$$

where the latter scaling is motivated by scaling arguments w.r.t. $\mathbf{w}$ and ν.

7. Numerical experiments. In this section, we will show some numerical experiments for the proposed method. The results demonstrate the accuracy of the stabilized TraceFEM and verify the analysis results on error estimates and condition number bounds.

All implementations are done in the finite element package DROPS [8]. We applied both the backward Euler scheme and the BDF2 scheme to approximate the time derivative. At each time step, we assemble the stiffness matrix and the right-hand side by numerical integration over the discrete surfaces Γ_h^n which is obtained by piecewise linear interpolation ϕ_h^n of the exact level set function ϕ^n, $\Gamma_h^n = \{\mathbf{x} \in \mathbb{R}^3 \ : \ \phi_h^n(\mathbf{x}) = 0\}$, i.e. $q = 1$ in (20). For the disretization in space we consider piecewise linears, i.e. $k = 1$ in (19). The computational domain in all considered examples is $\Omega = [-2, 2]^3$ which contains $\Gamma(t)$ (and $\Gamma_h(t)$) at all times $t \in [0, T]$. To arrive at a computation mesh, we use a combination of uniform subdivision into cubes with side length h and a Kuhn subdivision into 6 tetrahedra. This results in the shape regular background triangulation $\mathcal{T}_h$. The temporal grid is chosen uniform in all experiments, $t_n = n\Delta t$ with $\Delta t = \frac{T}{N}$. For the narrow band zone we choose $c_\delta = 2.5$ in (24) which is sufficient for the backward Euler and the BDF2 scheme. All linear systems are solved using GMRES with a Gauss–Seidel preconditioner to a relative tolerance of 10^{-15}.

In the experiments we are interested in the $L^2(0, T; H^1(\Gamma_h(t))$ and $L^2(0, T; L^2(\Gamma_h(t))$ surface norms for the error which we approximate using the trapezoidal quadrature rule in time. To investigate the rates of convergence we apply successive refinements in space and in time.

For the different test problems, below, we apply the backward Euler scheme and the BDF2 scheme. For reasons of compactness, only in the first experiment we apply the two different scalings for ρ_n, cf. (83), where we choose the constants so that $\rho_n = 4$ and $\rho_n = \frac{\nu}{\delta_h + h} + \|\mathbf{w}\|_\infty$ and evaluate errors as well as condition numbers. In the other experiments we only consider $\rho_n = \frac{\nu}{\delta_h + h} + \|\mathbf{w}\|_\infty$.

Experiment 1. We consider the transport–diffusion equation (1) on a unit sphere $\Gamma(t)$ moving with the constant velocity $\mathbf{w} = (0.2, 0, 0)$ for $t \in [0, T]$, $T = 1$. The level-set function ϕ,

$$\phi = |\mathbf{x} - \mathbf{c}(t)| - 1,$$

with $\mathbf{c}(t) = t\mathbf{w}$ describes a sphere with radius 1 that moves along $\mathbf{w}$. We notice that ϕ is a signed distance function. The initial data is given by

$$\Gamma^0 := \{\mathbf{x} \in \mathbb{R}^3 \ : \ |\mathbf{x}| = 1\}, \quad u(\mathbf{x}, 0) = 1 + x_1 + x_2 + x_3.$$

Table 2

Table 2

$L^2(H^1)$- and $L^2(L^2)$-norm error in Experiment 1 with backward Euler and $\rho_n = \|\mathbf{w}\|_\infty + \nu(\delta_h + h)^{-1}$.

	$L^2(H^1)$-norm of the error				$L^2(L^2)$-norm of the error			
	$h=1/2$	$h=1/4$	$h=1/8$	$h=1/16$	$h=1/2$	$h=1/4$	$h=1/8$	$h=1/16$
$\Delta t = 1/8$	$9.5\cdot 10^{-1}$	$6.0\cdot 10^{-1}$	$3.8\cdot 10^{-1}$	$2.5\cdot 10^{-1}$	$1.3\cdot 10^{-1}$	$1.0\cdot 10^{-1}$	$1.2\cdot 10^{-1}$	$1.3\cdot 10^{-1}$
$\Delta t = 1/32$	$9.2\cdot 10^{-1}$	$6.1\cdot 10^{-1}$	$3.5\cdot 10^{-1}$	$1.9\cdot 10^{-1}$	$1.8\cdot 10^{-1}$	$1.0\cdot 10^{-1}$	$3.1\cdot 10^{-2}$	$3.3\cdot 10^{-2}$
$\Delta t = 1/128$	$9.1\cdot 10^{-1}$	$6.2\cdot 10^{-1}$	$3.5\cdot 10^{-1}$	$1.8\cdot 10^{-1}$	$2.0\cdot 10^{-1}$	$1.2\cdot 10^{-1}$	$2.8\cdot 10^{-2}$	$8.3\cdot 10^{-3}$
$\Delta t = 1/512$	$9.1\cdot 10^{-1}$	$6.2\cdot 10^{-1}$	$3.6\cdot 10^{-1}$	$1.8\cdot 10^{-1}$	$2.0\cdot 10^{-1}$	$1.2\cdot 10^{-1}$	$3.1\cdot 10^{-2}$	$7.2\cdot 10^{-3}$

Table 3

Maximum condition number in Experiment 1 for two different choices for ρ_n.

	$\kappa(\mathbf{A})$ for $\rho_n = 4$					$\kappa(\mathbf{A})$ for $\rho_n = \|\mathbf{w}\|_\infty + \nu(\delta_h + h)^{-1}$			
	$h=1/2$	$h=1/4$	$h=1/8$	$h=1/16$		$h=1/2$	$h=1/4$	$h=1/8$	$h=1/16$
$\Delta t = 1/2$	$5.7\cdot 10^{1}$	$1.1\cdot 10^{2}$	$3.3\cdot 10^{2}$	$1.8\cdot 10^{3}$	$\Delta t = 1/2$	$1.8\cdot 10^{2}$	$2.4\cdot 10^{2}$	$4.8\cdot 10^{2}$	$2.1\cdot 10^{3}$
$\Delta t = 1/4$	$6.2\cdot 10^{1}$	$9.0\cdot 10^{1}$	$1.8\cdot 10^{2}$	$6.3\cdot 10^{2}$	$\Delta t = 1/4$	$1.9\cdot 10^{2}$	$1.7\cdot 10^{2}$	$2.3\cdot 10^{2}$	$7.4\cdot 10^{2}$
$\Delta t = 1/8$	$7.2\cdot 10^{1}$	$7.7\cdot 10^{1}$	$1.6\cdot 10^{2}$	$3.4\cdot 10^{2}$	$\Delta t = 1/8$	$2.3\cdot 10^{2}$	$1.7\cdot 10^{2}$	$1.8\cdot 10^{2}$	$3.3\cdot 10^{2}$
$\Delta t = 1/16$	$1.1\cdot 10^{2}$	$8.3\cdot 10^{1}$	$1.6\cdot 10^{2}$	$3.0\cdot 10^{2}$	$\Delta t = 1/16$	$3.6\cdot 10^{2}$	$1.8\cdot 10^{2}$	$1.7\cdot 10^{2}$	$2.1\cdot 10^{2}$
$\Delta t = 1/32$	$1.9\cdot 10^{2}$	$1.0\cdot 10^{2}$	$1.4\cdot 10^{2}$	$2.9\cdot 10^{2}$	$\Delta t = 1/32$	$6.7\cdot 10^{2}$	$2.2\cdot 10^{2}$	$1.7\cdot 10^{2}$	$1.7\cdot 10^{2}$
$\Delta t = 1/64$	$3.5\cdot 10^{2}$	$1.5\cdot 10^{2}$	$1.5\cdot 10^{2}$	$2.9\cdot 10^{2}$	$\Delta t = 1/64$	$1.3\cdot 10^{3}$	$3.3\cdot 10^{2}$	$1.7\cdot 10^{2}$	$1.6\cdot 10^{2}$
$\Delta t = 1/128$	$6.9\cdot 10^{2}$	$2.8\cdot 10^{2}$	$1.8\cdot 10^{2}$	$2.9\cdot 10^{2}$	$\Delta t = 1/128$	$2.6\cdot 10^{3}$	$6.1\cdot 10^{2}$	$2.0\cdot 10^{2}$	$1.7\cdot 10^{2}$

One easily checks that the exact solution is given by $u(\mathbf{x}, t) = 1 + (x_1 + x_2 + x_3 - 0.2t)\exp(-2t)$ and that $\xi = 0.1$ in (7). For sufficiently small h we can assume that $\xi_h \approx 0.1$ (cf, (51)) which ensures unique solvability of every time step for $\Delta t \leq 2$.

The error measures for the backward Euler method are shown in Tables 1 and Table 2 for the different scalings for ρ_n. In both cases we observe an $\mathcal{O}(h)$-convergence in the $L^2(H^1)$-norm. The initial temporal resolution is already so high that the spatial error is always dominating and we do not observe the linear convergence in time, yet. However, for the $L^2(L^2)$-norm we observe a convergence with $h^2 + \Delta t$. The impact of the scaling of ρ_n on the results is very small which can be seen as some robustness of the method (in view of accuracy) with respect to the stabilization parameter ρ_n.

The maximal condition numbers for each simulation are shown in Table 3 for the different scalings. We first discuss $\rho_n = 4$. For fixed $\Delta t = 1/2$, we observe that the condition number increases like $\mathcal{O}(h^{-2})$ which is slightly better than predicted. For fixed $h = 1/2$, the condition number increases with order $\mathcal{O}(\Delta t^{-1})$. When we refine h and Δt simultaneously, we observe the predicted $\mathcal{O}(h^{-1})$ behavior for both cases with $\Delta t \sim h$ and $\Delta t \sim h^2$. For the scaling $\rho_n = \|\mathbf{w}\|_\infty + \frac{\nu}{\delta_h + h}$ we observe slightly higher condition numbers, the same behavior for fixed h or fixed Δt, but a better scaling for $\Delta t \sim h$ and $\Delta t \sim h^2$. For $\Delta t \sim h$ the condition number only grows slowly with h^{-1} (not even linear as predicted) and is constant for $\Delta t \sim h^2$.

Finally, we do experiments for the BDF2 scheme, cf. Remark 5.2. In this case, we expect that the method is of $\mathcal{O}(\Delta t^2)$ accuracy. This is clearly shown in Table 4 when we refine both h and Δt (with $\Delta t \sim h$). In these tests, we only considered $\rho_n = 4$. We notice that the system matrix is different from that of the backward Euler scheme only by a different coefficient in front of the mass matrix. Therefore, the algebraic stability of the BDF2 scheme is the same as that of the backward Euler scheme, and is covered by the analysis in Section 6. These results indicate that the stabilized TraceFEM method can be generalized to higher order time discretization schemes.

Experiment 2. The setup of this experiment is similar to the previous one. The transport velocity is given by a standing vortex, $\mathbf{w} = (-0.2\pi x_2, 0.2\pi x_1, 0)$ for $t \in [0, T]$, $T = 1$. Initially, the sphere with radius 1 is located off the center. The initial data is

$$\Gamma^0 := \{\mathbf{x} \in \mathbb{R}^3 \ : \ |\mathbf{x} - \mathbf{x}_0| = 1\}, \quad u|_{t=0} = 1 + (x_1 - 0.5) + x_2 + x_3,$$

with $\mathbf{x}_0 = (0.5, 0, 0)$. As the level-set function we choose

$$\phi = (x_1 - 0.5\cos 0.2\pi t)^2 + (x_2 - 0.5\sin 0.2\pi t)^2 + x_3^2 - 1.$$

TABLE 4
$L^2(H^1)$- and $L^2(L^2)$-norm error in Experiment 1 with BDF2 scheme and $\rho_n = 4$.

	$L^2(H^1)$-norm of the error				$L^2(L^2)$-norm of the error			
	$h=1/2$	$h=1/4$	$h=1/8$	$h=1/16$	$h=1/2$	$h=1/4$	$h=1/8$	$h=1/16$
$\Delta t = 1/8$	$\underline{1.0}$	$6.8\cdot 10^{-1}$	$3.7\cdot 10^{-1}$	$1.9\cdot 10^{-1}$	$\underline{3.2\cdot 10^{-1}}$	$1.6\cdot 10^{-1}$	$4.3\cdot 10^{-2}$	$2.8\cdot 10^{-2}$
$\Delta t = 1/16$	$9.8\cdot 10^{-1}$	$\underline{6.7\cdot 10^{-1}}$	$3.6\cdot 10^{-1}$	$1.8\cdot 10^{-1}$	$3.1\cdot 10^{-1}$	$\underline{1.5\cdot 10^{-1}}$	$3.3\cdot 10^{-2}$	$1.3\cdot 10^{-2}$
$\Delta t = 1/32$	$9.5\cdot 10^{-1}$	$6.5\cdot 10^{-1}$	$\underline{3.6\cdot 10^{-1}}$	$1.8\cdot 10^{-1}$	$3.1\cdot 10^{-1}$	$1.5\cdot 10^{-1}$	$\underline{3.1\cdot 10^{-2}}$	$8.2\cdot 10^{-3}$
$\Delta t = 1/64$	$9.3\cdot 10^{-1}$	$6.5\cdot 10^{-1}$	$3.5\cdot 10^{-1}$	$\underline{1.8\cdot 10^{-1}}$	$3.1\cdot 10^{-1}$	$1.5\cdot 10^{-1}$	$3.1\cdot 10^{-2}$	$\underline{7.6\cdot 10^{-3}}$

TABLE 5
$L^2(H^1)$- and $L^2(L^2)$-norm error in Experiment 2 with backward Euler and $\rho_n = \|\mathbf{w}\|_\infty + \nu(\delta_h + h)^{-1}$.

	$L^2(H^1)$-norm of the error				$L^2(L^2)$-norm of the error			
	$h=1/2$	$h=1/4$	$h=1/8$	$h=1/16$	$h=1/2$	$h=1/4$	$h=1/8$	$h=1/16$
$\Delta t = 1/8$	$\underline{1.0}$	$6.5\cdot 10^{-1}$	$3.8\cdot 10^{-1}$	$3.4\cdot 10^{-1}$	$\underline{2.7\cdot 10^{-1}}$	$1.4\cdot 10^{-1}$	$1.5\cdot 10^{-1}$	$2.1\cdot 10^{-1}$
$\Delta t = 1/32$	$9.9\cdot 10^{-1}$	$\underline{6.5\cdot 10^{-1}}$	$3.5\cdot 10^{-1}$	$1.8\cdot 10^{-1}$	$2.9\cdot 10^{-1}$	$\underline{1.1\cdot 10^{-1}}$	$4.2\cdot 10^{-2}$	$4.0\cdot 10^{-2}$
$\Delta t = 1/128$	$9.9\cdot 10^{-1}$	$6.6\cdot 10^{-1}$	$\underline{3.5\cdot 10^{-1}}$	$1.8\cdot 10^{-1}$	$3.1\cdot 10^{-1}$	$1.2\cdot 10^{-1}$	$\underline{3.2\cdot 10^{-2}}$	$1.1\cdot 10^{-2}$
$\Delta t = 1/512$	$10.0\cdot 10^{-1}$	$6.6\cdot 10^{-1}$	$3.5\cdot 10^{-1}$	$\underline{1.8\cdot 10^{-1}}$	$3.2\cdot 10^{-1}$	$1.2\cdot 10^{-1}$	$3.4\cdot 10^{-2}$	$\underline{8.4\cdot 10^{-3}}$

which is not a signed distance function. Now $\mathbf{w}$ revolves the sphere around the center of the domain without changing its shape. One checks that the exact solution to (1) is given by

$$u(\mathbf{x}, t) = (x_1(\cos(0.2\pi t) - \sin(0.2\pi t)) + x_2(\cos(0.2\pi t) + \sin(0.2\pi t)) + x_3 + 0.5)\exp(-2t).$$

and that there hold the bounds $\xi \leq 0.6$ and $\|w_N\|_\infty \leq \frac{\pi}{10}$. Hence, for h sufficiently small $\Delta t \leq 0.4$ ensures unique solvability in every time step.

The numerical results are similar to those in Experiment 1. For simplicity, we show only the errors for the backward Euler scheme with $\rho_n = \|\mathbf{w}\|_\infty + \frac{\nu}{\delta_h + h}$ in Table 5. If one refines both Δt and h with constraint $\Delta t \sim h^2$, the first order of convergence in the surface $L^2(H^1)$-norm and the second order in the surface $L^2(L^2)$-norm with respect to h are again observed. This example demonstrates that the numerical method works well even if the level-set function is not a signed distance function.

Experiment 3. In this experiment, we consider a shrinking sphere and solve (1) with a source term on the right-hand side. The bulk velocity field is given by $\mathbf{w} = -\frac{3}{4}e^{-t/2}\mathbf{n}$, for $t \in [0, T]$, $T = 0.5$. Here $\mathbf{n}$ is the unit outward normal on $\Gamma(t)$. Γ^0 is the sphere with radius $r_0 = 1.5$. The level-set function is chosen as a signed distance function $\phi = |\mathbf{x}| - r(t)$, with $r(t) = r_0 e^{-t/2}$. One computes $\xi = -1$ and $\|w_N\|_\infty = \frac{3}{4}$ and with the right-hand side $f(\mathbf{x}, t) = (-1.5e^t + \frac{16}{3}e^{2t})x_1 x_2 x_3$. the exact solution $u(\mathbf{x}, t) = (1 + x_1 x_2 x_3)e^t$. Table 6 shows the error norms for various time steps Δt and mesh sizes h. The results are consistent with the previous experiments and our analysis.

Experiment 4. Additionally, we consider a problem where two initially separated spheres merge to only surface. The numerical results are similar to that by the method based on a fast matching extension in [39], i.e. a stable numerical solution. This indicates that proposed method is robust also problems with topology changes (which is not covered by our numerical analysis).

8. Conclusions and open problem. In this paper we introduced a new numerical method for PDEs for evolving surfaces on the example of a scalar transport diffusion equation. The main feature of the method is its simplicity. With the help of the stabilization which also provides a meaningful extension, standard time integration methods based on finite differences can be applied and combined with a TraceFEM for the spatial discretization. The two components, time and space discretizations can be exchanged so that higher order in space and/or in time methods can be used, if desired (and available). Besides the introduction of the method, we carried out a careful a priori error analysis yielding optimal order estimates and reasonable condition number bounds. For the accessibility of the paper we made several restrictions and simplifications. We mention aspects where we think that an extension of our results beyond these restrictions is worth pursuing.

The geometry in the analysis part of the paper is always described by a level set function which has the signed distance property. We made this assumption as it simplified the - still technical

TABLE 6
$L^2(H^1)$- and $L^2(L^2)$-norm error in Experiment 3 with backward Euler and $\rho_n = \|\mathbf{w}\|_\infty + \nu(\delta_h + h)^{-1}$.

	$L^2(H^1)$-norm of the error				$L^2(L^2)$-norm of the error			
	$h=1/2$	$h=1/4$	$h=1/8$	$h=1/16$	$h=1/2$	$h=1/4$	$h=1/8$	$h=1/16$
$\Delta t = 1/8$	$\underline{9.3\cdot 10^{-1}}$	$6.0\cdot 10^{-1}$	$3.4\cdot 10^{-1}$	$2.1\cdot 10^{-1}$	$\underline{1.5\cdot 10^{-1}}$	$8.5\cdot 10^{-2}$	$9.2\cdot 10^{-2}$	$1.1\cdot 10^{-1}$
$\Delta t = 1/32$	$9.2\cdot 10^{-1}$	$\underline{6.1\cdot 10^{-1}}$	$3.3\cdot 10^{-1}$	$1.7\cdot 10^{-1}$	$2.0\cdot 10^{-1}$	$\underline{7.6\cdot 10^{-2}}$	$2.7\cdot 10^{-2}$	$2.5\cdot 10^{-2}$
$\Delta t = 1/128$	$9.2\cdot 10^{-1}$	$6.2\cdot 10^{-1}$	$\underline{3.3\cdot 10^{-1}}$	$1.7\cdot 10^{-1}$	$2.2\cdot 10^{-1}$	$8.6\cdot 10^{-2}$	$\underline{2.2\cdot 10^{-2}}$	$7.1\cdot 10^{-3}$
$\Delta t = 1/512$	$9.2\cdot 10^{-1}$	$6.2\cdot 10^{-1}$	$3.3\cdot 10^{-1}$	$\underline{1.7\cdot 10^{-1}}$	$2.2\cdot 10^{-1}$	$8.8\cdot 10^{-2}$	$2.4\cdot 10^{-2}$	$\underline{5.8\cdot 10^{-3}}$

enough - analysis. However, we believe that this assumption could be replaced with the much milder assumption $c \le \|\nabla\phi\| \le c^{-1}$ for some $0 < c < 1$ in the vicinity of the surface.

The exponential growth in the a priori error analysis is due to the divergence term in (1) which is not sign definite. For a non-negative divergence or strong diffusion the exponential growth vanishes which can be used for improved stability and error bounds, cf. Remark 3.1.

Often practically relevant transport–diffusion equations are transport dominated. In these cases additional convection stabilizations may be desired. For stationary surfaces this can be dealt with a streamline–diffusion–type stabilization for TraceFEM as in [37] or a discontinuous Galerkin Trace-FEM discretization as in [4]. These techniques can be combined with our time marching method.

The analysis in this paper only treats the backward Euler time discretization method although the methodology allows for a larger class of time stepping schemes. In Remark 5.2 we also commented on adaptations of the analysis for a BDF2 scheme. The application and analysis of Crank–Nicolson or Runge–Kutta type schemes for this discretization has not been considered yet, but is an interesting natural extension of the method.

The a priori error results presented in section 5.5 give bounds for the error at fixed times and an $L^2(H^1)$-type bound in space–time using energy-type arguments. We expect that the application of duality techniques can improve these bounds yielding an additional order in space in weaker norms such as $L^2(L^2)$-type space–time norms.

The method and its analysis allow for higher order discretizations in space. However, the realisation of geometrically high order accurate discretizations is a non-trivial task, cf. Remark 4.1. A combination of recent developments in the accurate numerical integration on level set domains with this time discretization approach is an interesting topic for future research.

Finally, we are not aware of an analog of the presented approach for PDEs posed in evolving volumetric domains or volumetric domains with evolving interfaces. Moving in this directions would require new extension results for finite element functions for implicitly defined and geometrically unfitted domains. This is a topic of a forthcoming paper.

REFERENCES

[1] A. ALPHONSE, C. M. ELLIOTT, AND B. STINNER, *On some linear parabolic pdes on moving hypersurfaces*, Interfaces Free Bound., 17 (2015), pp. 157–187.
[2] M. BERTALMIO, L.-T. CHENG, S. OSHER, AND G. SAPIRO, *Variational problems and partial differential equations on implicit surfaces*, Journal of Computational Physics, 174 (2001), pp. 759–780.
[3] E. BURMAN, P. HANSBO, AND M. G. LARSON, *A stabilized cut finite element method for partial differential equations on surfaces: The Laplace–Beltrami operator*, Computer Methods in Applied Mechanics and Engineering, 285 (2015), pp. 188–207.
[4] E. BURMAN, P. HANSBO, M. G. LARSON, AND A. MASSING, *Cut finite element methods for partial differential equations on embedded manifolds of arbitrary codimensions*, arXiv preprint arXiv:1610.01660, (2016).
[5] J. W. CAHN, P. FIFE, AND O. PENROSE, *A phase field model for diffusion induced grain boundary motion*, Acta Mater, 45 (1997), pp. 4397–4413.
[6] K. DECKELNICK, C. M. ELLIOTT, AND T. RANNER, *Unfitted finite element methods using bulk meshes for surface partial differential equations*, SIAM Journal on Numerical Analysis, 52 (2014), pp. 2137–2162.
[7] A. DEMLOW AND G. DZIUK, *An adaptive finite element method for the Laplace-Beltrami operator on implicitly defined surfaces*, SIAM Journal on Numerical Analysis, 45 (2007), pp. 421–442.
[8] *DROPS package.* http://www.igpm.rwth-aachen.de/DROPS/.
[9] G. DZIUK AND C. M. ELLIOTT, *Finite elements on evolving surfaces*, IMA J. Numer. Anal., 27 (2007), pp. 262–292.
[10] ——, *Finite element methods for surface PDEs*, Acta Numerica, 22 (2013), pp. 289–396.

[11] C. M. ELLIOTT AND B. STINNER, *Modeling and computation of two phase geometric biomembranes using surface finite elements*, Journal of Computational Physics, 226 (2007), pp. 1271–1290.

[12] M. ELMAN, H.C. NAD SCHULTZ, *Preconditioning by fast direct methods for non-selfadjoint nonseparable elliptic equations*, SIAM Journal on Numerical Analysis, 12 (1986), pp. 44–56.

[13] C. ENGWER, T. RANNER, AND S. WESTERHEIDE, *An unfitted discontinuous galerkin scheme for conservation laws on evolving surfaces*, in Proceedings of ALGORITMY 2016, A. Handlovicova and D. Sevcovic, eds., 2016, pp. 44–54.

[14] T.-P. FRIES AND S. OMEROVI, *Higher-order accurate integration of implicit geometries*, International Journal for Numerical Methods in Engineering, (2015).

[15] J. GRANDE, *Eulerian finite element methods for parabolic equations on moving surfaces*, SIAM Journal on Scientific Computing, 36 (2014), pp. B248–B271.

[16] J. GRANDE, C. LEHRENFELD, AND A. REUSKEN, *Analysis of a high order trace finite element method for pdes on level set surfaces*, arXiv preprint arXiv:1611.01100, (2016).

[17] S. GROSS, M. A. OLSHANSKII, AND A. REUSKEN, *A trace finite element method for a class of coupled bulk-interface transport problems*, ESAIM: Mathematical Modelling and Numerical Analysis, 49 (2015), pp. 1303–1330.

[18] S. GROSS AND A. REUSKEN, *Numerical Methods for Two-phase Incompressible Flows*, Springer, Berlin, 2011.

[19] E. HAIRER AND G. WANNER, *Solving ordinary differential equations. II: Stiff and Differential Algebraic Problems*, Springer-Verlag, Berlin, 2002. second edition.

[20] A. HANSBO AND P. HANSBO, *An unfitted finite element method, based on Nitsche's method, for elliptic interface problems*, Comput. Methods Appl. Mech. Engrg., 191 (2002), pp. 5537–5552.

[21] P. HANSBO, M. G. LARSON, AND S. ZAHEDI, *Characteristic cut finite element methods for convection–diffusion problems on time dependent surfaces*, Computer Methods in Applied Mechanics and Engineering, 293 (2015), pp. 431–461.

[22] ———, *A cut finite element method for coupled bulk–surface problems on time–dependent domains*, Computer Methods in Applied Mechanics and Engineering, 307 (2016), pp. 96–116.

[23] A. JAMES AND J. LOWENGRUB, *A surfactant-conserving volume-of-fluid method for interfacial flows with insoluble surfactant*, J. Comp. Phys., 201 (2004), pp. 685–722.

[24] C. LEHRENFELD, *The Nitsche XFEM-DG space-time method and its implementation in three space dimensions*, SIAM J. Sci. Comp., 37 (2015), pp. A245–A270.

[25] ———, *High order unfitted finite element methods on level set domains using isoparametric mappings*, Comp. Meth. Appl. Mech. Eng., 300 (2016), pp. 716–733.

[26] C. LEHRENFELD AND A. REUSKEN, *Analysis of a high order unfitted finite element method for an elliptic interface problem*, arXiv preprint arXiv:1602.02970, (2016). accepted for publication in IMA JNA (2017).

[27] W. E. LORENSEN AND H. E. CLINE, *Marching cubes: A high resolution 3d surface construction algorithm*, in ACM SIGGRAPH Computer Graphics, vol. 21, ACM, 1987, pp. 163–169.

[28] U. F. MAYER AND G. SIMONNETT, *Classical solutions for diffusion induced grain boundary motion*, J. Math. Anal., 234 (1999), pp. 660–674.

[29] U. M. MAYER, A. GERSTENBERGER, AND W. A. WALL, *Interface handling for three-dimensional higher-order XFEM-computations in fluid–structure interaction*, International Journal for Numerical Methods in Engineering, 79 (2009), pp. 846–869.

[30] W. MILLIKEN, H. STONE, AND L. LEAL, *The effect of surfactant on transient motion of newtonian drops*, Phys. Fluids A, 5 (1993), pp. 69–79.

[31] B. MÜLLER, F. KUMMER, AND M. OBERLACK, *Highly accurate surface and volume integration on implicit domains by means of moment-fitting*, International Journal for Numerical Methods in Engineering, 96 (2013), pp. 512–528.

[32] I. L. NOVAK, F. GAO, Y.-S. CHOI, D. RESASCO, J. C. SCHAFF, AND B. SLEPCHENKO, *Diffusion on a curved surface coupled to diffusion in the volume: application to cell biology*, Journal of Computational Physics, 229 (2010), pp. 6585–6612.

[33] M. A. OLSHANSKII AND A. REUSKEN, *Error analysis of a space–time finite element method for solving PDEs on evolving surfaces*, SIAM Journal on Numerical Analysis, 52 (2014), pp. 2092–2120.

[34] ———, *Trace finite element methods for PDEs on surfaces*, arXiv preprint arXiv:1612.00054, (2016).

[35] M. A. OLSHANSKII, A. REUSKEN, AND J. GRANDE, *A finite element method for elliptic equations on surfaces*, SIAM Journal on Numerical Analysis, 47 (2009), pp. 3339–3358.

[36] M. A. OLSHANSKII, A. REUSKEN, AND X. XU, *An eulerian space–time finite element method for diffusion problems on evolving surfaces*, SIAM Journal on Numerical Analysis, 52 (2014), pp. 1354–1377.

[37] ———, *A stabilized finite element method for advection-diffusion equations on surfaces*, IMA J Numer Math, (2014).

[38] M. A. OLSHANSKII AND D. SAFIN, *Numerical integration over implicitly defined domains for higher order unfitted finite element methods*, Lobachevskii Journal of Mathematics, 37 (2016), pp. 582–596.

[39] M. A. OLSHANSKII AND X. XU, *A trace finite element method for pdes on evolving surfaces*, SIAM Journal on Scientific Computing, 39 (2017), pp. A1301–A1319.

[40] A. REUSKEN, *Analysis of trace finite element methods for surface partial differential equations*, IMA Journal of Numerical Analysis, 35 (2015), pp. 1568–1590.

[41] R. SAYE, *High-order quadrature method for implicitly defined surfaces and volumes in hyperrectangles*, SIAM Journal on Scientific Computing, 37 (2015), pp. A993–A1019.

[42] H. STONE, *A simple derivation of the time-dependent convective-diffusion equation for surfactant transport along a deforming interface*, Phys. Fluids A, 2 (1990), pp. 111–112.

[43] Y. SUDHAKAR AND W. A. WALL, *Quadrature schemes for arbitrary convex/concave volumes and integration of*

weak form in enriched partition of unity methods, Computer Methods in Applied Mechanics and Engineering, 258 (2013), pp. 39–54.

[44] J.-J. Xu and H.-K. Zhao, An Eulerian formulation for solving partial differential equations along a moving interface, Journal of Scientific Computing, 19 (2003), pp. 573–594.